

# MASSIV: Mass Assembly Survey with SINFONI in VVDS<sup>★</sup>

## V. The major merger rate of star-forming galaxies at $0.9 < z < 1.8$ from IFS-based close pairs

C. López-Sanjuan<sup>1,2</sup>, O. Le Fèvre<sup>1</sup>, L. A. M. Tasca<sup>1</sup>, B. Epinat<sup>1,3,4</sup>, P. Amram<sup>1</sup>, T. Contini<sup>3,4</sup>, B. Garilli<sup>5</sup>, M. Kissler-Patig<sup>6</sup>, J. Moutaka<sup>3,4</sup>, L. Paioro<sup>5</sup>, V. Perret<sup>1</sup>, J. Queyrel<sup>3,4</sup>, L. Tresse<sup>1</sup>, D. Vergani<sup>7</sup>, and C. Divoy<sup>3,4</sup>

<sup>1</sup> Aix Marseille Université, CNRS, LAM (Laboratoire d'Astrophysique de Marseille) UMR 7326, 13388, Marseille, France

<sup>2</sup> Centro de Estudios de Física del Cosmos de Aragón, Plaza San Juan 1, planta 2, 44001, Teruel, Spain  
e-mail: c1s@cefca.es

<sup>3</sup> Institut de Recherche en Astrophysique et Planétologie (IRAP), CNRS, 14 avenue Édouard Belin, 31400, Toulouse, France

<sup>4</sup> IRAP, Université de Toulouse, UPS-OMP, Toulouse, France

<sup>5</sup> IASF-INAF, via Bassini 15, 20133, Milano, Italy

<sup>6</sup> ESO, Karl-Schwarzschild-Str.2, 85748, Garching b. München, Germany

<sup>7</sup> INAF-IAAFBO, Via P. Gobetti 101, 40129 Bologna, Italy

Received 24 August 2012 / Accepted 10 March 2013

### ABSTRACT

*Context.* The contribution of the merging process to the early phase of galaxy assembly at  $z > 1$  and, in particular, to the build-up of the red sequence, still needs to be accurately assessed.

*Aims.* We aim to measure the major merger rate of star-forming galaxies at  $0.9 < z < 1.8$ , using close pairs identified from integral field spectroscopy (IFS).

*Methods.* We use the velocity field maps obtained with SINFONI/VLT on the MASSIV sample, selected from the star-forming population in the VVDS. We identify physical pairs of galaxies from the measurement of the relative velocity and the projected separation ( $r_p$ ) of the galaxies in the pair. Using the well constrained selection function of the MASSIV sample, we derive at a mean redshift up to  $z = 1.54$  the gas-rich major merger fraction (luminosity ratio  $\mu = L_2/L_1 \geq 1/4$ ), and the gas-rich major merger rate using merger time scales from cosmological simulations.

*Results.* We find a high gas-rich major merger fraction of  $20.8^{+15.2}_{-6.8}\%$ ,  $20.1^{+8.0}_{-5.1}\%$ , and  $22.0^{+13.7}_{-7.3}\%$  for close pairs with  $r_p \leq 20h^{-1}$  kpc in redshift ranges  $z = [0.94, 1.06]$ ,  $[1.2, 1.5]$ , and  $[1.5, 1.8]$ , respectively. This translates into a gas-rich major merger rate of  $0.116^{+0.084}_{-0.038} \text{ Gyr}^{-1}$ ,  $0.147^{+0.058}_{-0.037} \text{ Gyr}^{-1}$ , and  $0.127^{+0.079}_{-0.042} \text{ Gyr}^{-1}$  at  $z = 1.03, 1.32$ , and  $1.54$ , respectively. Combining our results with previous studies at  $z < 1$ , the gas-rich major merger rate evolves as  $(1+z)^n$ , with  $n = 3.95 \pm 0.12$ , up to  $z = 1.5$ . From these results we infer that  $\sim 35\%$  of the star-forming galaxies with stellar masses  $\overline{M}_* = 10^{10} - 10^{10.5} M_\odot$  have undergone a major merger since  $z \sim 1.5$ . We develop a simple model that shows that, assuming that all gas-rich major mergers lead to early-type galaxies, the combined effect of gas-rich and dry mergers is able to explain most of the evolution in the number density of massive early-type galaxies since  $z \sim 1.5$ , with our measured gas-rich merger rate accounting for about two-thirds of this evolution.

*Conclusions.* Merging of star-forming galaxies is frequent at around the peak in star formation activity. Our results show that gas-rich mergers make an important contribution to the growth of massive galaxies since  $z \sim 1.5$ , particularly on the build-up of the red sequence.

**Key words.** galaxies:evolution — galaxies:formation — galaxies:interactions

## 1. Introduction

Understanding the mechanisms involved in the mass assembly of galaxies and their relative role over cosmic time is an important open topic in modern astrophysics. In particular, the evolution of the red sequence, which includes passive galaxies dominated by old stellar populations and an early-type (E/SO) morphology,

imposes fundamental constraints on the formation and evolution models.

The stellar mass density in the red sequence has increased by a factor of  $\sim 10$  in the 2.5 Gyr between  $z = 2$  and  $z = 1$ , but only by a factor of  $\sim 2$  in the last 7 – 8 Gyr of cosmic history (e.g., Arnouts et al. 2007; Vergani et al. 2008; Ilbert et al. 2010). Major mergers, the merger of two galaxies with similar stellar masses, is an efficient mechanism for creating new passive, early-type galaxies (e.g., Naab et al. 2006; Rothberg & Joseph 2006a,b; Hopkins et al. 2008; Rothberg & Fischer 2010; Bournaud et al. 2011). Thus, the knowledge of the merger rate at  $z > 1$  is important input when estimating the relative contribution of merging and cold-gas accretion (e.g., Dekel & Birnboim 2006) in the early assem-

<sup>★</sup> This work is based mainly on observations collected at the European Southern Observatory (ESO) Very Large Telescope (VLT), Paranal, Chile, as part of the Programs 179.A-0823, 177.A-0837, 78.A-0177, 75.A-0318, and 70.A-9007. This work also benefits from data products produced at TERAPIX and the Canadian Astronomy Data Centre as part of the Canada-France-Hawaii Telescope Legacy Survey, a collaborative project of NRC and CNRS.

bly of galaxies and, in particular, the role of merging in the build-up of the red sequence.

The evolution of the merger rate since  $z \sim 1$  is now well constrained by direct observations. The early measurements using photometric pairs (Patton et al. 1997; Le Fèvre et al. 2000) or post-merger morphological signatures (Conselice 2003; Jogee et al. 2009) have been superseded by spectroscopic measurements confirming physical pairs from the redshift measurement of both components of a major merger with a luminosity/mass ratio  $\mu \geq 1/4$  (e.g., Lin et al. 2008; de Ravel et al. 2009, 2011), as well as for minor mergers down to  $\mu = 1/10$  (López-Sanjuan et al. 2011). With a parametrization of the merger rate's evolution following  $\propto (1+z)^n$ , it is observed that the major merger rate's evolution depends on the luminosity and on the mass of the galaxy sample (e.g., de Ravel et al. 2009), where massive galaxies with  $M_\star > 10^{11} M_\odot$  have a higher merger rate, but with little redshift evolution ( $n \sim 0-2$ ), while lower mass galaxies with  $M_\star = 10^9 - 10^{11} M_\odot$  have a lower merging rate but with stronger redshift evolution ( $n \sim 3-4$ ). This mass dependency seems to explain some of the apparent discrepancy of merger rate measurements made from observations targeting different mass samples.

Beyond  $z \sim 1$ , direct measurements of the merger rate are still limited. Previous attempts to measure the major merger rate at  $z > 1$  have focused on the identification of merger remnants from morphological signatures (Conselice et al. 2008, 2011b; Bluck et al. 2012), on the study of projected close pairs (Ryan et al. 2008; Bluck et al. 2009; Williams et al. 2011; Man et al. 2012; Mármol-Queraltó et al. 2012; Law et al. 2012), or on indirect estimations (Cameron & Pettitt 2012; Puech et al. 2012). These studies find a high merger rate to  $z \sim 2-3$  but with a large scatter between different measurements. However, these results are up to now solely based on photometric measurements which are increasingly hard to correct for contamination along the line of sight as redshift increases. Another complication stems from the morphological evolution of galaxies, with show more irregular morphologies at high redshifts, and a wavelength dependency with more multi-component objects present when observed in the rest-frame UV (Law et al. 2007), with some of these components possibly related to strong star-forming regions rather than to different dynamical components.

To improve on this situation, it is necessary to obtain spectroscopic confirmation of the physical nature of the photometric pairs at  $z \gtrsim 1$ . In the last years, NIR Integral Field Spectrographs (IFSs), like SINFONI on the VLT or OSIRIS on the Keck, have opened the possibility for a systematic study of the dynamical field around high redshift galaxies in the optical rest-frame. Some examples are the MASSIV<sup>1</sup> (Mass Assembly Survey with SINFONI in VVDS, Contini et al. 2012) survey at  $0.9 < z < 1.8$ , the SINS<sup>2</sup> (Spectroscopic Imaging survey in the Near-infrared with SINFONI, Förster Schreiber et al. 2009) survey at  $z \sim 2$ , or the Keck-OSIRIS (Law et al. 2009), the AMAZE (Assessing the Mass-Abundance redshift -Z- Evolution, Maiolino et al. 2008) and the LSD (Lyman-break galaxies Stellar populations and Dynamics, Mannucci et al. 2009) surveys at  $z \sim 3$ .

The MASSIV survey has been designed to target the peak of the star-formation rate at  $0.9 < z < 1.8$ , filling the gap between higher redshift ( $z \sim 2$ ) IFS surveys with those at  $z < 1$ , e.g., IMAGES (Intermediate MAss Galaxy Evolution Sequence, Yang et al. 2008). The MASSIV survey has targeted 84 star-forming galaxies at  $0.9 < z < 1.8$  with SINFONI, drawn

from the VVDS<sup>3</sup> (VIMOS VLT Deep Survey, Le Fèvre et al. 2005) survey. MASSIV has been used as a unique opportunity to study in detail the dynamical state of  $0.9 < z < 1.8$  galaxies (Epinat et al. 2012), their metallicity gradients (Queyrel et al. 2012), or the evolution of the fundamental mass-size-velocity relations since  $z \sim 1.2$  (Vergani et al. 2012).

In this paper, using the MASSIV survey, we present for the first time a measurement of the gas-rich major merger rate of star-forming galaxies from kinematical close pairs at  $0.9 < z < 1.8$ . Thanks to the large field-of-view of IFS we have access to the complete surrounding volume of the galaxies when searching for close kinematical companions. In addition, the well-defined selection of sources from the VVDS and the well controlled selection function of MASSIV observations ensures the study of a representative population of star-forming galaxies at these redshifts (see Contini et al. 2012, for details). This all together enables the measurement of average volume quantities like the merger fraction and rate.

The paper is organised as follows: in Sect. 2 we summarise the MASSIV data set used to identify merging pairs, and in Sect. 3 we develop the methodology to measure the merger fraction from IFS data. We report the gas-rich major merger fraction in MASSIV in Sect. 4, and derive the gas-rich major merger rate in Sect. 5. We discuss the implication of our results in Sect. 6. Finally, we present our conclusions in Sect. 7. We use  $H_0 = 100h$  km s<sup>-1</sup> Mpc<sup>-1</sup>,  $h = 0.7$ ,  $\Omega_m = 0.3$ , and  $\Omega_\Lambda = 0.7$  throughout this paper. All magnitudes refer to the AB system. The stellar masses assume a Salpeter (1955) initial mass function (IMF).

## 2. The MASSIV data set

The galaxy sample studied in this paper is the final release of the MASSIV project (ESO Large Programme 179.A-0823; PI.: T. Contini). A full description of the sample can be found in Contini et al. (2012). We briefly summarise some properties of this sample of 84 galaxies below. The galaxies were selected from the VVDS in the RA = 2h area of the deep ( $I_{AB} \leq 24$ ; Le Fèvre et al. 2005) and ultradeep ( $I_{AB} \leq 24.75$ ; Le Fèvre et al., in prep.) surveys, and in the RA = 14h and RA = 22h areas of the wide survey ( $I_{AB} \leq 22.5$ ; Garilli et al. 2008).

The MASSIV sources are a subsample of the VVDS star-forming population at  $z > 0.9$ . The star-forming selection was performed on the measured intensity of [O II] $\lambda 3727$  emission line in the VIMOS spectrum (see Lamareille et al. 2009; Vergani et al. 2008) or, for the cases where the [O II] $\lambda 3727$  emission line was out of the VIMOS spectral range (i.e., for  $z \gtrsim 1.5$  galaxies), on the UV flux based on their observed photometric *UBVR*K spectral energy distribution and/or UV rest-frame spectrum. The star formation criteria ensure that rest-frame optical emission lines H $\alpha$  and [N II] $\lambda 6584$ , or in a few cases [O III] $\lambda 5007$ , will be bright enough to be observed with SINFONI in the NIR *J* (sources at  $z < 1.1$ ) and *H* (sources at  $z > 1.1$ ) bands. In addition, to ensure that the H $\alpha$  emission line will be detected with SINFONI with a sufficient signal-to-noise (*S/N*) ratio in a reasonable exposure time, an additional selection in the [O II] $\lambda 3727$  equivalent width of  $0.9 < z < 1.5$  sources is imposed. The final selection of parent VVDS star-forming galaxies in the [O II] $\lambda 3727$  flux vs equivalent width plane at  $0.9 < z < 1.5$  is shown in Fig. 1.

The 84 MASSIV sources were randomly selected from the star-forming population in the VVDS and also fulfil two important observational constraints, (i) the observed wavelength of

<sup>1</sup> <http://www.ast.obs-mip.fr/users/contini/MASSIV/>

<sup>2</sup> [http://www.mpe.mpg.de/forster/SINS/sins\\_nmf.html](http://www.mpe.mpg.de/forster/SINS/sins_nmf.html)

<sup>3</sup> <http://cesam.oamp.fr/vvdsproject/>

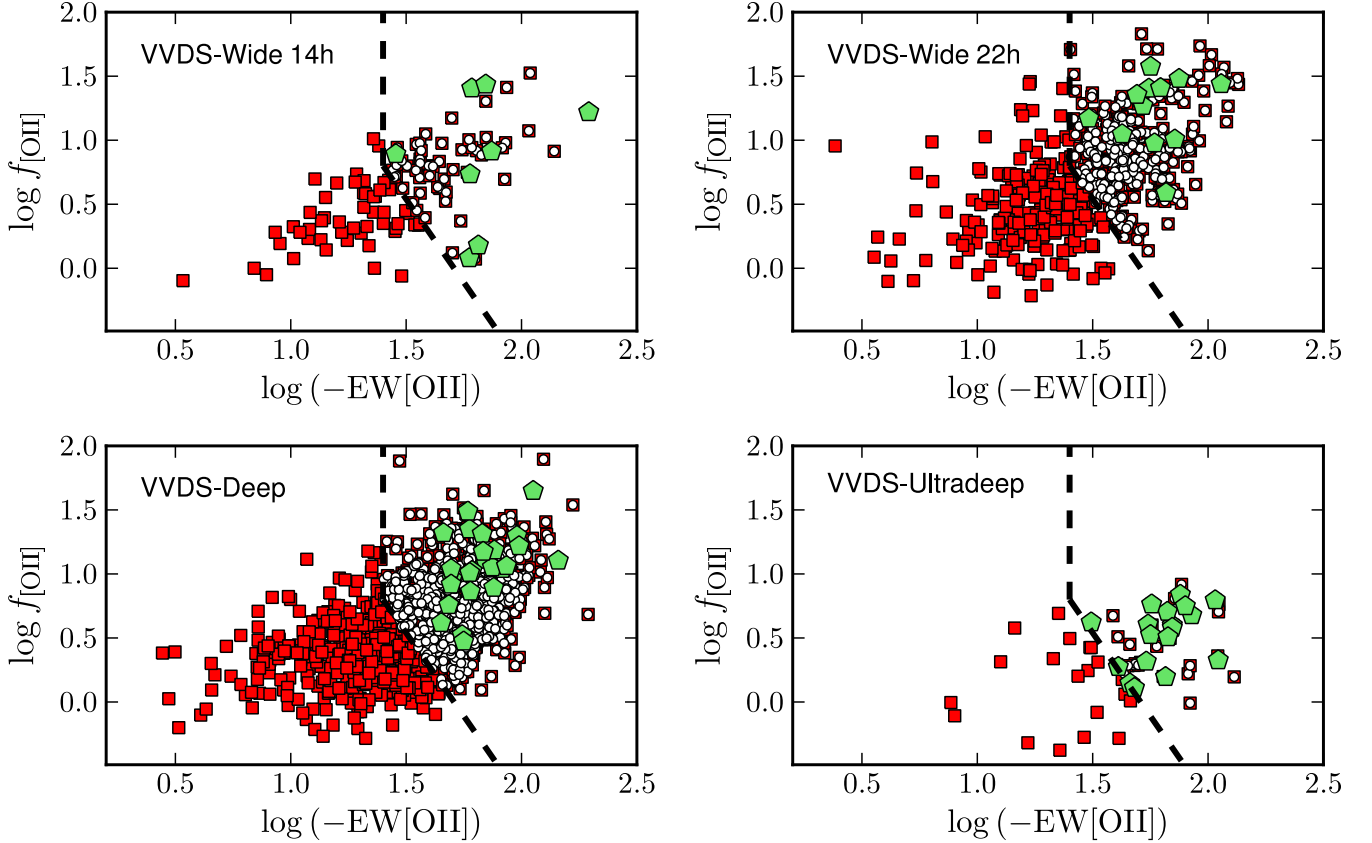


**Fig. 1.** MASSIV selection in the  $[\text{O II}]\lambda 3727$  flux [ $10^{-17}$  erg  $\text{s}^{-1}$   $\text{cm}^{-2}$ ] vs equivalent width [ $\text{\AA}$ ] plane (see Contini et al. 2012, for details). Red squares are the VVDS sources at  $0.94 < z < 1.5$  with individual  $[\text{O II}]\lambda 3727$  line measurement in the VVDS-Wide 14h (top-left), VVDS-Wide 22h (top-right), VVDS-Deep (bottom-left), and VVDS-Ultradeep surveys (bottom-right). The dashed lines mark the selection of MASSIV star-forming galaxies. White dots are those VVDS sources that fulfil the MASSIV selection. Green pentagons are the MASSIV galaxies observed with SINFONI/VLT. [A colour version of this plot is available at the electronic edition].

$H\alpha$  line falls  $9\text{\AA}$  away from strong OH night-sky lines, in order to avoid heavy contamination of the galaxy spectrum by sky-subtraction residuals. And (ii) a bright star ( $R < 18$  mag) is close enough to the target to observe it at higher spatial resolution with the adaptive optics (AO) system of SINFONI.

The most stringent selection criterion used to build the MASSIV sample is certainly the requirement of a minimum  $[\text{O II}]\lambda 3727$  equivalent width. This sensitivity limit is likely to translate into an overall bias towards younger and more actively star-forming systems. To check for this possible effect, Contini et al. (2012) compare the properties of the MASSIV sample with those of the global VVDS sample, which is purely apparent magnitude-selected without any colour selection and thus representative of the overall star-forming population of galaxies at high redshifts. They conclude that the final MASSIV sample provides a good representation of “normal” star-forming galaxies at  $0.9 < z < 1.8$  in the stellar mass regime  $M_{\star} = 10^9 - 10^{11} M_{\odot}$ , with a median star formation rate  $SFR \sim 30 M_{\odot} \text{ yr}^{-1}$  and a detection limit of  $\sim 5 M_{\odot} \text{ yr}^{-1}$ .

The observations have been performed between April 2007 and January 2011. Most (85%) of the galaxies in the sample have been observed in a seeing-limited mode (with a spatial sampling of 0.125 arcsec/pixel). However, eleven galaxies have been acquired with AO assisted with a laser guide star (AO/LGS, seven with 0.05 and four with 0.125 arcsec/pixel spatial sampling). The data reduction was performed with the ESO SINFONI pipeline

(version 2.0.0), using the standard master calibration files provided by ESO. The absolute astrometry for the SINFONI data cubes was derived from nearby bright stars also used for point spread function (PSF) measurements. Custom IDL and Python scripts have been used to flux calibrate, align, and combine all the individual exposures. For each galaxy a non sky-subtracted cube was also created, mainly to estimate the effective spectral resolution. For more details on data reduction, we refer to Epinat et al. (2012).

We use the  $H\alpha$  emission line (or  $[\text{O III}]\lambda 5007$  in a few cases) in the SINFONI data cubes to derive the kinematical maps (flux, velocity field and velocity dispersion map) of the MASSIV galaxies. To estimate their dynamical properties, we assume that the ionised gas rotates in a thin disc with two regimes for the rotation velocity, a solid body shape in the innermost regions and a plateau in the outskirts. Using a  $\chi^2$  minimization we produce seeing-corrected velocity and dispersion maps of galaxies with geometrical inputs weighted for the  $S/N$  ratio of each pixel. We estimate the geometrical parameters used in the fitting model on the  $i$ -band best-seeing CFHTLS Megacam images for all galaxies (Goranova et al. 2009), except for VVDS-Wide 14h galaxies that were covered with the CFHT-12K/CFHT camera (Le Fèvre et al. 2004). We use the GALFIT software (Peng et al. 2002) that convolves a PSF with a model galaxy image based on the initial parameter estimates fitting a Sérsic (1968) profile. Residual maps from the fitting were used to optimise the results.

At the end of the fitting procedure, GALFIT converges into a final set of parameters such as the centre, the position angle, and the axial ratio. The  $i$ -band images were also used to correct for SINFONI astrometry, using the relative position of the PSF star. The morphology and kinematics maps of the 50 first-epoch galaxies are presented in Epinat et al. (2012) together with a more extensive discussion on the model fitting procedure. The 34 second-epoch galaxies, already included in the present work, will be presented in a future paper.

We obtain the stellar mass of MASSIV galaxies from a spectral energy distribution (SED) fit to the photometric and spectroscopic data with Bruzual & Charlot (2003) stellar population synthesis models using the GOSSIP2 Spectral Energy Distribution tool (Franzetti et al. 2008). We assume a Salpeter (1955) IMF, and a set of delayed exponential star formation histories with galaxy ages in the range from 0.1 to 15 Gyr. As input for the SED fitting, in addition to the VVDS spectra, we use the multi-band photometric observations available in the VVDS fields (see Contini et al. 2012, for further details). Following Walcher et al. (2008) we adopt the probability distribution function to obtain the stellar mass.

In all, the final 84 MASSIV galaxies are representative of the normal star-forming ( $SFR \gtrsim 5M_{\odot} \text{ yr}^{-1}$ ) population of  $M_{\star} = 10^9 - 10^{11} M_{\odot}$  galaxies at  $0.9 < z < 1.8$ .

### 3. Measuring the merger fraction from IFS data

We define as a close pair two galaxies with a projected separation in the sky plane  $r_p^{\min} \leq r_p \leq r_p^{\max}$  and a rest-frame relative velocity along the line of sight  $\Delta v \leq \Delta v^{\max}$ . We used  $\Delta v^{\max} = 500 \text{ km s}^{-1}$  and  $r_p^{\max} = 20 - 30 h^{-1} \text{ kpc}$  (see Sect. 3.3, for details), while setting  $r_p^{\min} = 0$ . We therefore searched for close companions in the kinematical maps of the MASSIV sources, analysing and classifying the sample using the velocity field and the velocity dispersion map (see Epinat et al. 2012, for details about the classification). Note that spectroscopic redshifts from the VVDS sources outside MASSIV are not used in this close pair search and only those sources detected in the SINFONI data cubes are taken into account. We find 20 close pair candidates in the MASSIV data cubes, and we study these systems in detail to select major (luminosity difference between both components  $\mu = L_2/L_1 \geq 1/4$ ) close pairs (Sect. 4).

If there was  $N_p$  major close pairs in our sample, the major merger fraction is

$$f_{\text{MM}} = \frac{N_p}{N}, \quad (1)$$

where  $N$  is the number of principal galaxies targeted for the survey. We named principal galaxy the source in the pair closest to the kinematical centre of the targeted system, even if it is not the brightest/more massive galaxy in the pair. In addition, we assume that all our close pairs are gas-rich: as shown by Vergani et al. (2012), the gas fraction of the MASSIV sources is above 10%, with a median value of  $\sim 30\%$ . The simple definition in Eq. (1) is only valid for volume-limited samples. While our sample is not only luminosity-limited but spectroscopically defined, we must take into account the different selection effects, both in the VVDS parent samples and in MASSIV, in our computation of the merger fraction.

#### 3.1. Accounting for selection effects in the VVDS

Since a fraction of the total number of potential targets in the VVDS fields have been spectroscopically observed and since

the redshifts are not measured with 100% accuracy, we must correct for the VVDS Target Sampling Rate ( $TSR$ ) and the Redshift Success Rate ( $SSR$ ), computed as a function of redshift and source magnitude. The  $SSR$  has been assumed independent of galaxy type, as demonstrated up to  $z \sim 1$  in Zucca et al. (2006). Every VVDS source has a redshift confidence flag (see Le Fèvre et al. 2005, for details), that can be flag = 4 (redshift 99% secure), flag = 3 (97% secure), flag = 2 (87% secure), flag = 9 (redshift from a single emission line, 90% secure), flag = 1 (50% secure), or flag = 0 (no redshift information). As several VVDS-Deep galaxies with flag = 2 have been re-observed in the VVDS-Ultradeep survey, providing a robust measurement of their redshift, this offers the opportunity to estimate the reliability of VVDS-Deep flag = 2 sources. We thus define a weight  $w_{29}$  to take this into account. We also define the weight  $w_{29}$  for flag = 9 sources by comparison with the latest photometric redshifts in the VVDS-Deep field (see Cucciati et al. 2010, for details about the latest photometric data set in the 2h field). By definition, the  $w_{29}$  weight is equal to 1 for flag = 3 and 4 sources in VVDS-Deep, and for all sources in VVDS-Wide and VVDS-Ultradeep. We derived the spectroscopic completeness weight for each galaxy  $i$  in the VVDS catalogue as

$$w_{\text{VVDS}}^i(z, I_{\text{AB}}, \text{flag}) = \frac{w_{29}^i(z, I_{\text{AB}}, \text{flag})}{TSR^i(z, I_{\text{AB}}) \times SSR^i(z, I_{\text{AB}})}. \quad (2)$$

The  $TSR$ ,  $SSR$  and  $w_{29}$  on VVDS-Deep and VVDS-Ultradeep were measured in previous works (Ilbert et al. 2006; Cucciati et al. 2012). We assume  $TSR = 0.22$  in VVDS-Wide fields (Garilli et al. 2008), and we detail the computation of the  $SSR$  in VVDS-Wide fields in Appendix A.

#### 3.2. Accounting for selection effects in the MASSIV survey

The MASSIV sources were randomly drawn from the star-forming population in the VVDS (Sect. 2). We correct for three basic selection effects in MASSIV.

- The selection weight,  $w_{\text{sel}}$ . We define this weight as the fraction of star-forming galaxies that fulfil the MASSIV selection in the  $[\text{O II}]\lambda 3727$  flux [ $10^{-17} \text{ erg s}^{-1} \text{ cm}^{-2}$ ] vs equivalent width [ $\text{\AA}$ ] plane at  $z < 1.5$  (Fig. 1). The weight  $w_{\text{sel}}$  tells us how representative the MASSIV selection of the global star-forming population in each of the VVDS surveys (Wide, Deep and Ultradeep) is, and gives more importance to the more representative samples. The VVDS-Deep and Ultradeep have  $w_{\text{sel}} \sim 0.67$  at  $z < 1.5$ , while the VVDS-Wide fields have  $w_{\text{sel}} \sim 0.53$  in the same redshift range. We assume  $w_{\text{sel}} = 1$  at  $z \geq 1.5$ , where the selection is based on colour/spectral properties and all the star-forming galaxies in the VVDS are thus pre-selected;
- the MASSIV IFS Rate ( $MIR$ ) is defined as the fraction of galaxies that fulfil the MASSIV selection and which were finally observed with SINFONI (Fig. 1). The  $MIR$  ranges from 0.43 for VVDS-Ultradeep to 0.05 for VVDS-Deep;
- the MASSIV Success Rate ( $MSR$ ) is the fraction of observed sources with a reliable kinematical classification. This fraction is always high,  $MSR \gtrsim 0.8$ .

Finally, the MASSIV weight is

$$w_{\text{MASSIV}}^j(x, z) = \frac{w_{\text{sel}}(x, z)}{MIR^j(x, z) \times MSR^j(x, z)}, \quad (3)$$

where the index  $j$  spans for the MASSIV sources and  $x$  refers to the VVDS survey (Wide at 14h, Wide at 22h, Deep or Ultradeep) to which the source belongs.

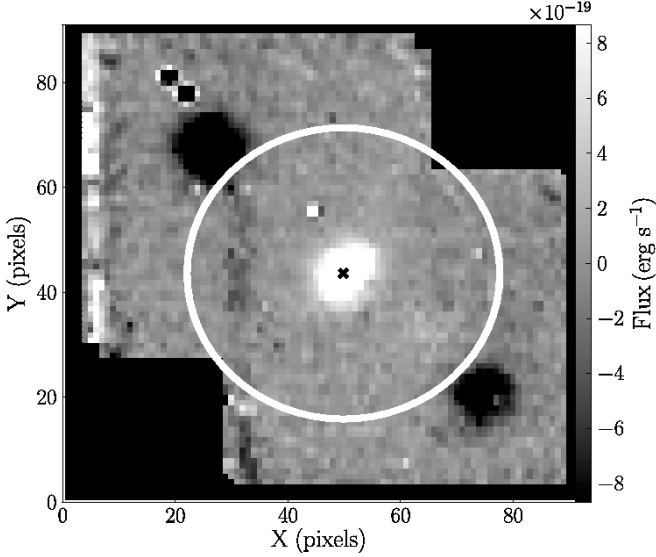


**Fig. 2.** Typical field-of-view of a MASSIV source. We show the flux of the source 220397579 in the five channels of its reduced, flux calibrated, data cube centred on the position of the  $H\alpha$  emission line (scale in the right). The pixel spatial scale is  $0.125''$ , that at the redshift of the source ( $z = 1.0379$ ) corresponds to  $\sim 1$  kpc. The source is at the centre of the image (black cross), while the white circle delimits the  $20h^{-1}$  kpc area around the source. In this particular case, 99% of this area is covered with MASSIV data and the two negatives of the source (black regions) are also excluded.

### 3.3. Area correction

Thanks to the large field-of-view of SINFONI, we have access to the complete surrounding volume of the principal galaxy when searching for close companions. This is a major advantage with respect to long-slit spectroscopic surveys, in which the observed number of close pairs is proportional to  $TSR^2$ , diminishing the statistics. However, the final reduced MASSIV data cubes cover a finite area in the sky plane. To deal with this, we define the area weight as

$$w_{\text{area}}^j(z, r_p^{\text{max}}) = \frac{A_r}{A_{\text{MASSIV}}}, \quad (4)$$

where  $A_r$  is the area subtended in the sky plane by a circle of radius  $r_p^{\text{max}}$  at the redshift of the source  $j$ , and  $A_{\text{MASSIV}}$  is the area of the same circle covered by the reduced SINFONI mosaic (Fig. 2). We state that the optimum search radius is  $r_p^{\text{max}} = 20h^{-1}$  kpc. This choice of  $r_p^{\text{max}}$  minimises the area correction, with  $w_{\text{area}} \sim 1$  in all cases. In addition, the two negatives of the main source produced by the offset observing procedure and that appear in the extremes of the reduced SINFONI mosaic are then excluded from the search area.

Finally, the corrected gas-rich major merger fraction is

$$f_{\text{MM}} = \frac{\sum_k^{N_p} w_{\text{VVDS}}^k w_{\text{MASSIV}}^k w_{\text{area}}^k}{\sum_j^N w_{\text{VVDS}}^j w_{\text{MASSIV}}^j}, \quad (5)$$

where the index  $j$  and  $k$  spans respectively for all MASSIV galaxies and for the MASSIV galaxies with a major close companion. The error budget in the major merger fraction is dominated by the low statistics. We use the Bayesian approach from Cameron (2011) to measure the statistical error in the raw major

merger fraction, i.e., in  $N_p/N$ , then scale it with the weighting scheme above.

## 4. Mergers classification and the gas-rich major merger fraction in MASSIV

In this section we measure, for the first time, the major merger fraction at  $0.9 < z < 1.8$  from spectroscopically-confirmed close pairs. The MASSIV observational strategy defines three natural redshift bins (Sect. 2). The low redshift MASSIV sources were observed in the  $J$  band, while the higher redshift ones in the  $H$  band. This translates to a gap in the redshift distribution at  $z \sim 1.1$ . In addition, the selection function of MASSIV targets changes at  $z = 1.5$ , providing another redshift boundary. We take advantage of these natural separations in the data to estimate the gas-rich major merger fraction in three redshift ranges,  $z_{r,1} = [0.94, 1.06]$ ,  $z_{r,2} = [1.2, 1.5)$ , and  $z_{r,3} = [1.5, 1.8)$ . We restrict our study to those galaxies with  $I_{\text{AB}} \leq 23.9$  to ensure completeness in the detection of close pairs (see Appendix C, for details).

We follow the steps described below to split the close pairs candidates in the MASSIV data cubes into major and no major mergers:

1. As described in Epinat et al. (2012), we had performed a classification of the MASSIV sources based on the shape of the velocity field (regular or irregular) and the close environment (isolated or not-isolated). From this classification, we had pre-selected as close pair candidates the non-isolated sources and those identified as mergers from the velocity field (see Epinat et al. 2012, for more details). We identified 20 close pair candidates (Table 1).
2. To study in detail these close pair candidates we used the deepest  $i$ -band images in the VVDS fields: CFTH12K (14h field, exposure time of  $t_{\text{exp}} = 3.6$  ks, Le Fèvre et al. 2004), CFHTLS-Wide (22h field,  $t_{\text{exp}} = 4 - 10$  ks, Goranova et al. 2009), and CFHTLS-Deep (02h field,  $t_{\text{exp}} \sim 300$  ks, Goranova et al. 2009). We run SExtractor on the systems with well separated sources, and GALFIT (with two Sérsic components) on the blended ones, to estimate the luminosity difference in the  $i$  band between both sources,  $\Delta m_i = m_{i,2} - m_{i,1}$ . We took  $\Delta m_i \leq 1.5$  (factor four or less in luminosity) to identify major mergers. The observed  $i$  band corresponds to  $\sim 300 - 350$  nm rest-frame in the redshift range of our sample. We stress that for the blended sources, we run GALFIT v3.0 (Peng et al. 2010) without imposing any constraint to the parameters of the fit and we only used the information from the kinematical maps to set the initial positions of the sources. We present the residual maps of these blended sources in Appendix B.
3. We confronted the images and the two component fits from GALFIT with the velocity field and the velocity dispersion map of the sources. We compared the distribution of  $H\alpha$  emission and the geometry of the velocity field to the rest-frame UV continuum (or rest-frame visible when NIR images are available). The presence of two components with position and geometry concordant in the velocity field and in the continuum images, is a strong indication of the reality of the pair.
4. We run SExtractor in the residual image from GALFIT with the principal source subtracted to obtain a second estimation of  $m_{i,2}$ , while with the companion source subtracted to estimate  $m_{i,1}$ . Then we compared the  $\Delta m_i$  derived from the GALFIT modeling with that from these SExtractor estimations. We found good agreement between both measure-

**Table 1.** Close pair candidates at  $0.9 < z < 1.8$  in the MASSIV sample.

ID	$z$	$r_p$ ( $h^{-1}$ kpc)	$\Delta v$ ( $\text{km s}^{-1}$ )	$\Delta m_i$	$\Delta m_{K_s}$	Classification
020294045	1.0028	2.9	180	0.4	0.3	<b>Major merger</b>
020386743	1.0487	3.7	80	1.8	...	No major merger
020461235	1.0349	2.8	15	1.7	...	No major merger
140096645	0.9655	...	...	> 1.5	...	No major merger
220397579	1.0379	14.4	340	0.4	-1.4	<b>Major merger</b>
220544394	1.0101	7.1	50	1.3	...	<b>Major merger</b>
020167131	1.2246	15.2	130	0.2	0.1	<b>Major merger</b>
020218856	1.3103	...	...	> 1.5	...	No major merger
020240675	1.3270	...	...	> 1.5	...	No major merger
020283083	1.2818	3.8	5	0.7	...	<b>Major merger</b>
020283830	1.3949	8.5	500	1.9	...	No major merger
020465775	1.3583	3.6	40	0.7	...	<b>Major merger</b>
220376206	1.2445	13.4	400	2.4	...	No major merger
220544103	1.3973	5.0	75	-1.1	...	<b>Major merger</b>
910154631	1.3347	4.2	130	0.8	...	<b>Major merger</b>
910296626	1.3558	12.1	165	-0.1	-0.2	<b>Major merger</b>
910337228	1.3955	9.5	220	1.4	...	<b>Major merger</b>
020116027	1.5302	26.8	100	0.7	0.5	<b>Major merger</b>
910186191	1.5399	12.7	450	-0.2	-2.4	<b>Major merger</b>
910274060	1.5694	3.4	10	0.2	...	<b>Major merger</b>

ments (difference of  $\sim 0.2$  mag or less). The major merger classification did not change from the initial estimate.

- Finally, we also explored  $\Delta m_{K_s}$  for well separated galaxies and for one blended source (020294045). We used the  $K_s$ -band images from UKIDSS-DXS survey (22h field, Dye et al. 2006) and WIRDS (2h field, Bielby et al. 2012). The observed  $K_s$  band corresponds to  $\sim 0.8-1 \mu\text{m}$  rest-frame in the redshift range of our sample, and is a better tracer of the stellar mass content of the galaxies. After this second check there is not change in the major merger classification, except for one close pair (source 910186191), supporting the previous  $i$ -band results.

We converged to the steps above after exploring different possibilities. The stellar mass ratio between the two galaxies in a close pair is the best parameter to classify such system as a major merger. However, the estimation of the stellar mass in the blended sources and in some well separated pairs is not feasible due to spatial resolution and photometric depth limitations. We concluded that the luminosity difference in the  $i$  band is an homogeneous criterion applicable to the whole MASSIV sample and have additional benefits (i) the observed  $i$  band corresponds to the UV continuum of the source, which is related with the star formation of the galaxy and thus with its  $H\alpha$  emission. Hence, both pieces of information should provide a consistent picture about the system under study. (ii) The MASSIV PSF is  $0.5 - 0.8''$ , similar to the typical seeing in the  $i$  band,  $\sim 0.74''$ , minimising spatial resolution differences. (iii) The  $3\sigma$  detection magnitude of the CFTLHS  $i$ -band images in the 2h field is  $\sim 26$  (AB). Thanks to this depth we are able to detect the outskirts of the fainter MASSIV galaxies, making feasible the decomposition of the blended sources. We tried the two components fit in redder bands, but the lower  $S/N$  lead in general to poor constraints. And (iv) the VVDS parent samples are  $i$ -band magnitude selected, so the completeness of the MASSIV close pair sample is well defined in the  $i$  band (see Appendix C, for further

details). In conclusion, even if  $\Delta m_i$  is not the optimal parameter to select major merger systems, it is the best practical one with the current data sets.

In the next sections we present the decomposition and the classification of the 20 close pair candidates in the MASSIV data cubes (Table 1).

#### 4.1. Close pair candidates at $0.94 \leq z \leq 1.06$

The weighted mean redshift of the first redshift bin is  $\bar{z}_{r,1} = 1.03$ . We have identified 6 close pairs over 18 sources in this redshift range:

- 020294045 (Fig. 3). **Major merger.** The velocity map suggests two projected components. The companion is toward the north and presents a steep velocity gradient compared with the principal galaxy. The GALFIT model with two components in the  $i$  band reproduces both the position of the two kinematical components in the velocity map and the high velocity dispersion in the overlapping region between both components. The luminosity difference is  $\Delta m_i = 0.4$ . The separation between the sources is  $2.9h^{-1}$  kpc and their relative velocity is  $\Delta v \sim 180 \text{ km s}^{-1}$ . Despite the close separation lead into significant overlap, this system also gives a satisfactory fit in the WIRDS  $K_s$ -band image (Fig.4). In this case  $\Delta m_{K_s} = 0.3$ , confirming that this system is a major merger.
- 020386743 (Fig. 5). *No major merger.* The velocity map suggests two projected components. The companion is toward the north and presents a different velocity than the northern part of the principal galaxy. The GALFIT model with two components suggests that we are only detecting the western part of the companion galaxy, with the eastern part being too faint. This is also consistent with the velocity dispersion map, which shows a regular pattern in the overlapping region. The separation between the sources is  $3.7h^{-1}$  kpc and



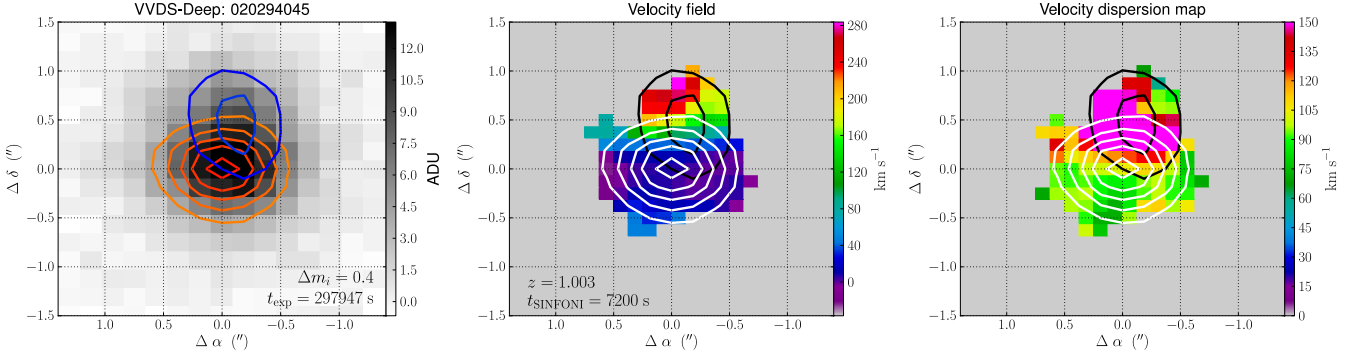


**Fig. 3.** The  $i$ -band image (*left panel*, scale in ADU in the right), the velocity field (*central panel*, scale in  $\text{km s}^{-1}$  in the right), and the velocity dispersion map (*right panel*, scale in  $\text{km s}^{-1}$  in the right) of the MASSIV source 020294045 (major merger). On each map, North is up and East is left. The level contours mark the isophotes of the two components obtained with GALFIT in the  $i$ -band image. The principal galaxy (red/white) is the one closer to the kinematical centre of the system and sets the origin in right ascension ( $\alpha$ ) and declination ( $\delta$ ), while the companion (blue/black) is the secondary component. The outer contour marks the 3.43 ADU ( $7\sigma_{\text{sky}}$ ) isophote. The next contours mark brighter isophotes in 1.96 ADU ( $4\sigma_{\text{sky}}$ ) steps. The luminosity difference between both components in the  $i$  band,  $\Delta m_i$ , as well as the CFHTLS exposure time,  $t_{\text{exp}}$ , are shown in the left panel. The redshift of the source and the on-source SINFONI exposure time,  $t_{\text{SINFONI}}$ , are shown in the central panel. [A colour version of this plot is available at the electronic edition].

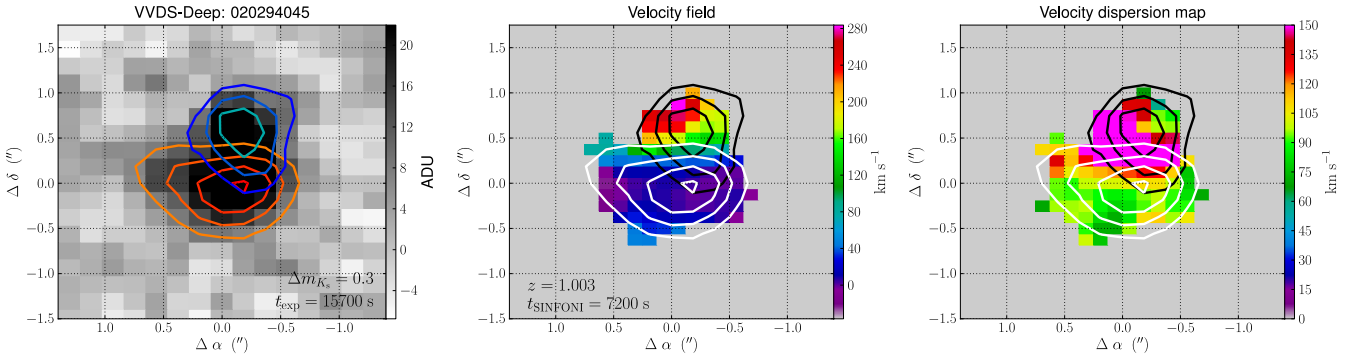


**Fig. 4.** The same as Fig. 3, but for the  $K_s$ -band image (*left panel*) of the MASSIV source 020294045 (major merger). The outer contour marks the 6.76 ADU ( $2\sigma_{\text{sky}}$ ) isophote, while brighter isophotes increase in 5.07 ADU ( $1.5\sigma_{\text{sky}}$ ) steps. The flux difference between both components in the  $K_s$  band,  $\Delta m_{K_s}$ , as well as the WIRDS exposure time,  $t_{\text{exp}}$ , are shown in the left panel. [A colour version of this plot is available at the electronic edition].

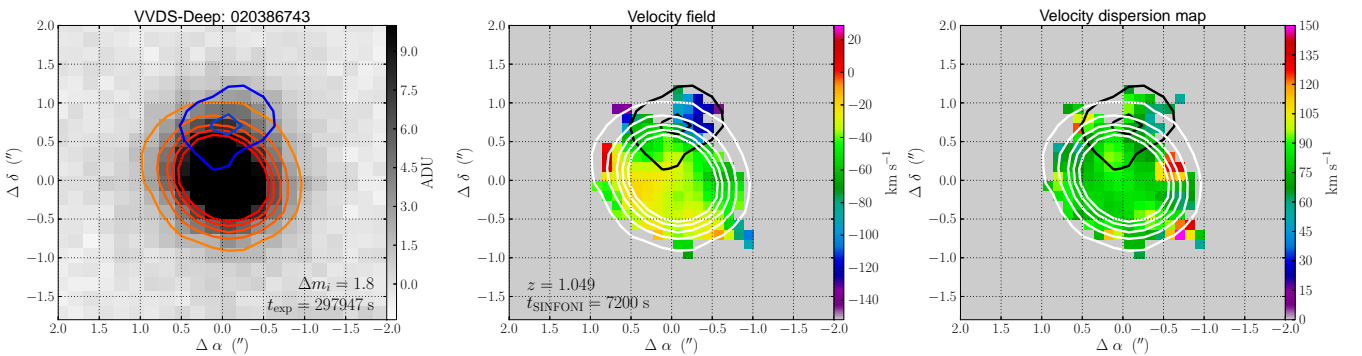


**Fig. 5.** The same as Fig. 3, but for the MASSIV source 020386743 (no major merger). The outer contour marks the 1.41 ADU ( $2\sigma_{\text{sky}}$ ) isophote, while brighter isophotes increase in 1.76 ADU ( $2.5\sigma_{\text{sky}}$ ) steps up to 10 ADU to avoid crowded figures. [A colour version of this plot is available at the electronic edition].

the luminosity difference is  $\Delta m_i = 1.8$ . Hence, we do not classify the system as a major merger.

- 020461235 (Fig. 6). *No major merger.* The velocity map suggests two projected components. The companion is to-

ward the south-west and presents a nearly constant velocity, in contrast with the velocity gradient of the principal galaxy. The GALFIT model with two components suggests that the companion is highly distorted, perhaps because the system is

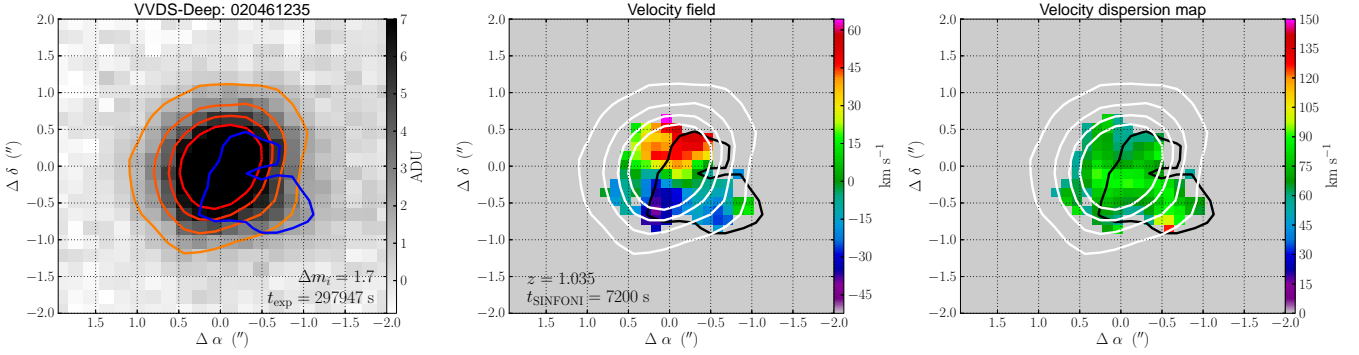


**Fig. 6.** The same as Fig. 3, but for the MASSIV source 020461235 (no major merger). The outer contour marks the 1.31 ADU ( $3\sigma_{\text{sky}}$ ) isophote, while brighter isophotes increase in 1.75 ADU ( $4\sigma_{\text{sky}}$ ) steps up to 7 ADU to avoid crowded figures. [A colour version of this plot is available at the electronic edition].

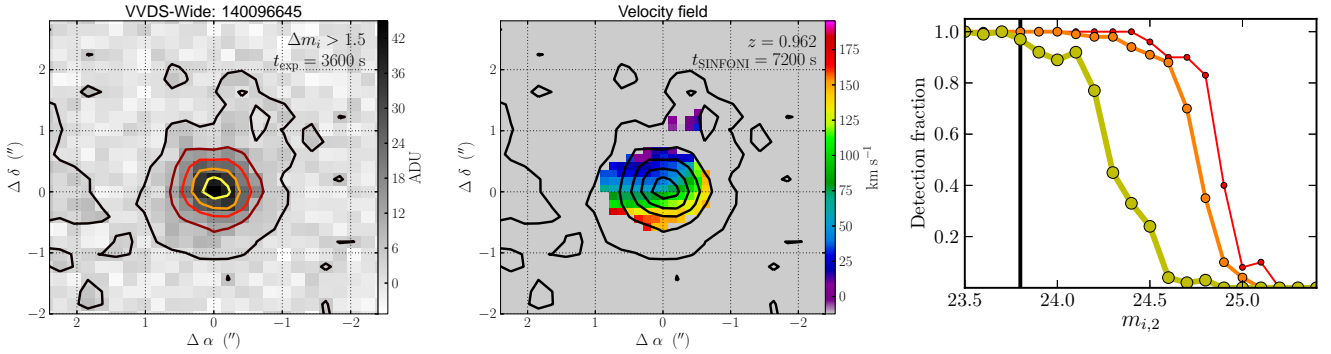


**Fig. 7.** Left and central panels are the same as in Fig. 3, but for the MASSIV source 140096645 (no major merger). The level contours mark the isophotes of the original  $i$ -band image. The  $H\alpha$  companion source is not detected in the  $i$  band. The outer contour marks the 2.64 ADU ( $1\sigma_{\text{sky}}$ ) isophote, while brighter isophotes increase in 7.94 ADU ( $3\sigma_{\text{sky}}$ ) steps up to 45 ADU to avoid crowded figures. The right panel shows the detection fraction of fake galaxies injected in the  $i$ -band image as a function of the magnitude of the companion source  $m_{i,2}$ . The size of the dots marks the detection curves for extended, normal and compact galaxies (see text for details). The vertical line marks the limiting magnitude for major companion ( $\Delta m_i = 1.5$ ). [A colour version of this plot is available at the electronic edition].

in an advanced merger stage (i.e., after first pericenter passage or pre-coalescence). The luminosity difference from the GALFIT model is  $\Delta m_i = 1.7$ , while from the residual maps is  $\Delta m_i = 1.9$ . This difference strongly suggests that this system is not a major merger. The separation between the components is  $2.8h^{-1}$  kpc.

- 140096645 (Fig. 7). *No major merger.* A small companion is identified in the velocity map about 1.2 arcsec away from the principal galaxy. There is no continuum detection in the  $i$ -band image in the position of the  $H\alpha$  companion, although there is a  $\sim 1\sigma_{\text{sky}}$  excess emission. To estimate if the non-detected companion could be bright/massive enough to lead to a major merger, we injected fake companion sources in the  $i$ -band image and studied their detection fraction as a function of the fake companion luminosity  $m_{i,2}$ . The fake sources were modelled with a Sérsic function and convolved with a typical PSF of the 14h field using GALFIT. For each fake source we assumed a random inclination and position angle, a Sérsic index  $n_s = 1$ , i.e., an exponential disc (we checked that the detection curve is similar assuming either  $n_s = 0.5$  or  $n_s = 2$ ), and an effective radius  $r_e$  given by the  $r_e - M_\star$  relation in MASSIV,  $\log r_e = 0.36 + 0.37[\log(M_\star/M_\odot) - 10]$  (see also Vergani et al. 2012). To estimate the stellar mass of the fake companion, we took  $\Delta m_i$  as a proxy of the mass ra-

tio between the principal galaxy, for which the stellar mass is known, and the companion. Then, we applied Poissonian noise to the model and injected it in the expected position of the possible companion. We measured, for different luminosities  $m_{i,2}$ , which fraction of the 500 injected fake sources were detected. We repeated the previous steps for fake sources with  $2r_e$  (extended sources) and  $0.5r_e$  (compact sources), spanning all the possible sizes of the real sources. We show the result of this experiment in the right panel of Fig. 7.

We find that even for extended sources, we are  $\sim 90\%$  complete at  $m_{i,2} \sim 24$ , while the limiting magnitude for a major companion is  $m_{i,2}^{\text{MM}} = 23.8$  (vertical line in the right panel of Fig. 7). Because of the small probability of non detection of a major companion, we classify this system as no major merger.

- 220397579 (Fig. 8). **Major merger.** The velocity map shows two different components with a separation of  $r_p = 14.4h^{-1}$  kpc and a relative velocity of  $\Delta v \sim 340$  km s $^{-1}$ . The companion is toward the north-west. The luminosity difference is  $\Delta m_i = 0.4$ , suggesting a major merger. The difference in the  $K_s$  band is  $\Delta m_{K_s} = -1.4$ . The negative sign implies that the companion is more luminous than the principal, which is brighter in the NUV rest-frame and in  $H\alpha$ . This is consistent



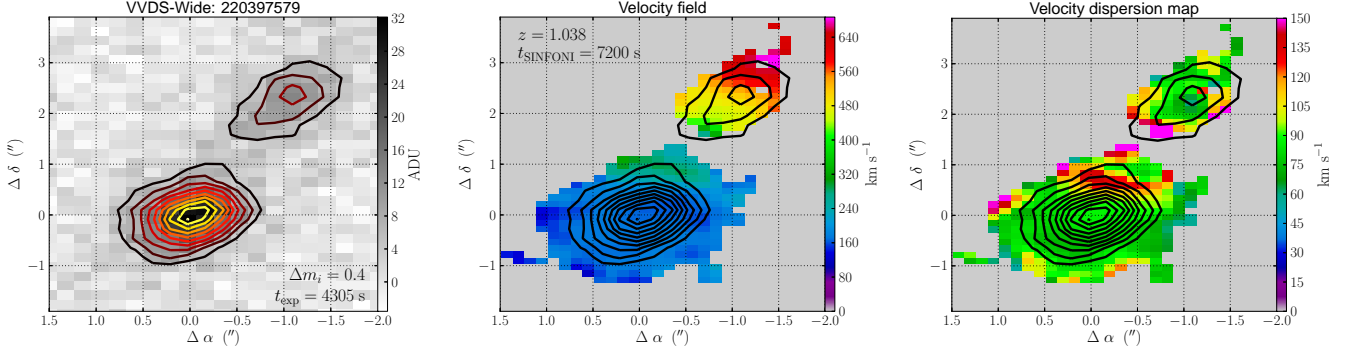


**Fig. 8.** The same as Fig. 3, but for the MASSIV source 220397579 (major merger). The level contours mark the isophotes of the original  $i$ -band image. The outer contour marks the 5.36 ADU ( $3\sigma_{\text{sky}}$ ) isophote, while brighter isophotes increase in 2.68 ADU ( $1.5\sigma_{\text{sky}}$ ) steps. [A colour version of this plot is available at the electronic edition].

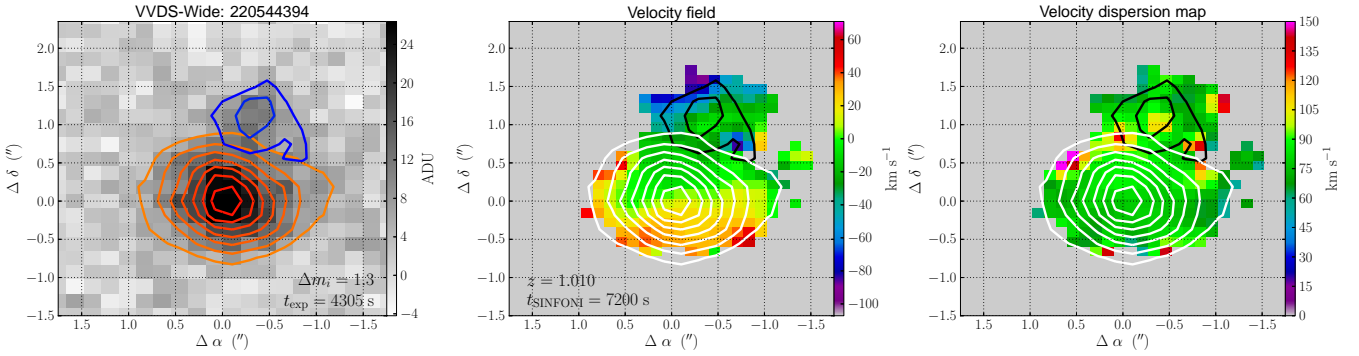


**Fig. 9.** The same as Fig. 3, but for the MASSIV source 220544394 (major merger). The outer contour marks the 4.31 ADU ( $2\sigma_{\text{sky}}$ ) isophote, while brighter isophotes increase in 3.23 ADU ( $1.5\sigma_{\text{sky}}$ ) steps. [A colour version of this plot is available at the electronic edition].

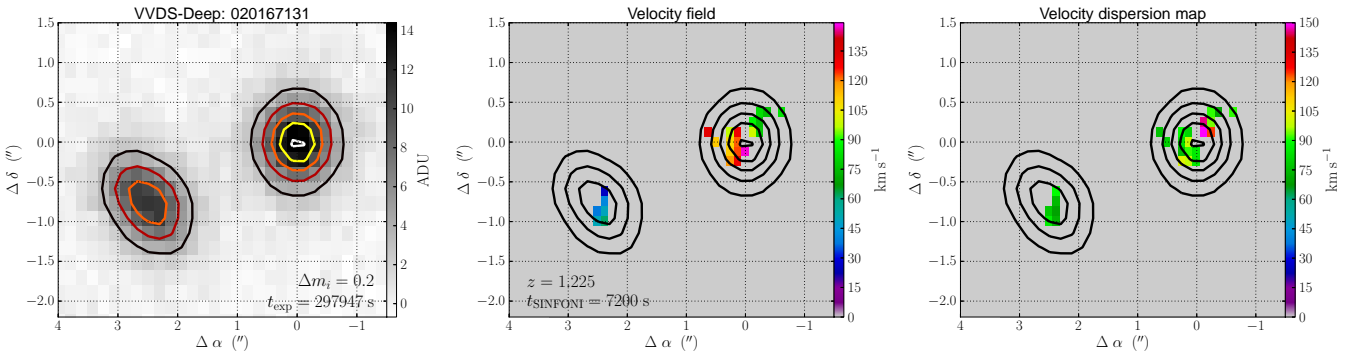


**Fig. 10.** The same as Fig. 8, but for the MASSIV source 020167131 (major merger). The outer contour marks the 3.43 ADU ( $10\sigma_{\text{sky}}$ ) isophote, while brighter isophotes increase in 2.74 ADU ( $8\sigma_{\text{sky}}$ ) steps. [A colour version of this plot is available at the electronic edition].

with the measured integrated metallicity of these sources, that is higher for the companion (Queyrel et al. 2012). The suggested picture is that the system comprises a nearly face-on principal galaxy with intense star formation and low dust reddening, and a nearly edge-on companion galaxy with either a low level of star formation or strong dust reddening. We classify the system as a major merger.

- 220544394 (Fig. 9). **Major merger.** The velocity map shows two different components with a separation of  $r_p = 7.1h^{-1}$  kpc and a relative velocity of  $\Delta v \sim 50 \text{ km s}^{-1}$ , that are also well recovered by the GALFIT model with two components.

The companion is toward the north, while the luminosity difference is  $\Delta m_i = 1.3$ . We classify the system as a major merger.

In summary for this redshift range, we classify 3 of the 6 close pair candidates as major mergers. This translates to a gas-rich major merger fraction of  $f_{\text{MM}} = 0.208^{+0.152}_{-0.068}$  at  $\bar{z}_{r,1} = 1.03$ .

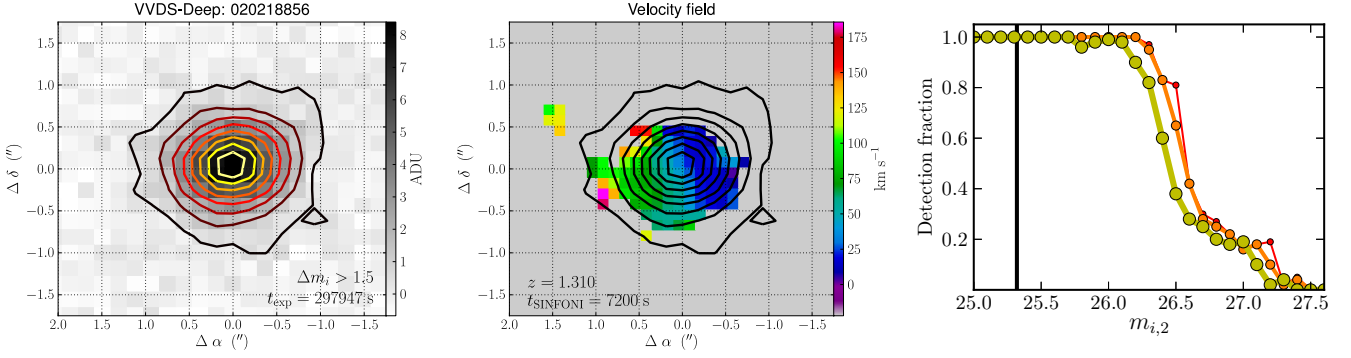


**Fig. 11.** The same as Fig. 7, but for the MASSIV source 020218856 (no major merger). The  $H\alpha$  companion galaxy is not detected in the  $i$  band. The outer contour marks the  $0.34$  ADU ( $1\sigma_{\text{sky}}$ ) isophote, while brighter isophotes increase in  $1.01$  ADU ( $3\sigma_{\text{sky}}$ ) steps. [A colour version of this plot is available at the electronic edition].

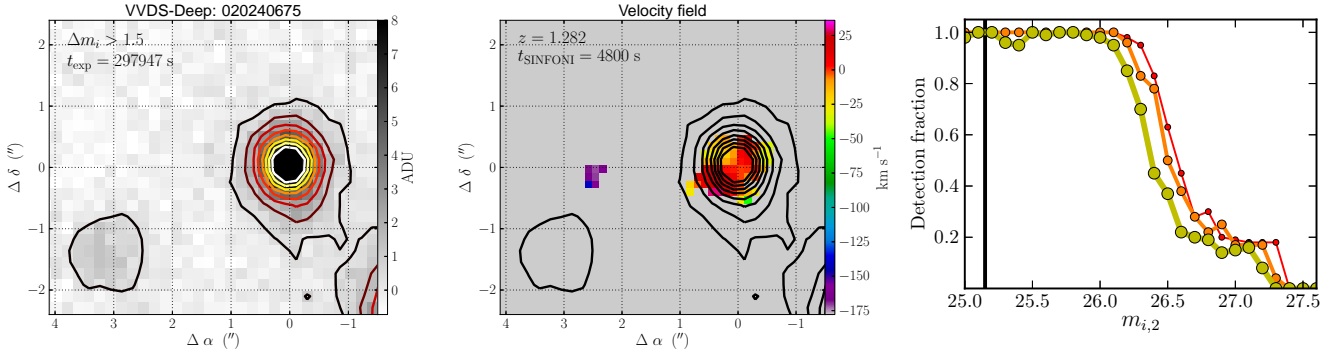


**Fig. 12.** The same as Fig. 7, but for the MASSIV source 020240675 (no major merger). The  $H\alpha$  companion galaxy is not detected in the  $i$  band. The outer contour marks the  $0.36$  ADU ( $1\sigma_{\text{sky}}$ ) isophote, while brighter isophotes increase in  $1.08$  ADU ( $3\sigma_{\text{sky}}$ ) steps up to  $8$  ADU to avoid crowded figures. [A colour version of this plot is available at the electronic edition].

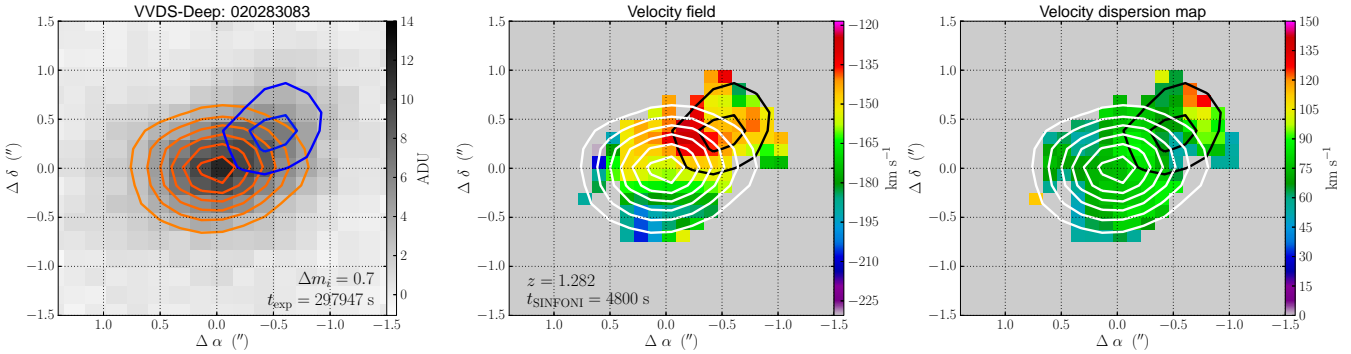


**Fig. 13.** The same as Fig. 3, but for the MASSIV source 020283083 (major merger). The outer contour marks the  $2.12$  ADU ( $4\sigma_{\text{sky}}$ ) isophote, while brighter isophotes increase in  $1.06$  ADU ( $2\sigma_{\text{sky}}$ ) steps. [A colour version of this plot is available at the electronic edition].

#### 4.2. Close pair candidates at $1.2 \leq z < 1.5$

The weighted mean redshift of the second redshift bin is  $\bar{z}_{r,2} = 1.32$ . This is a redshift range where there is no measurement of the major merger fraction from spectroscopic close pairs yet. In this framework, MASSIV provides an unique opportunity to measure the major merger fraction at this crucial epoch of galaxy evolution. We identify 11 close pair candidates over 30 galaxies in this redshift bin:

- 020167131 (Fig. 10). **Major merger.** The velocity map shows two different components with a separation of  $r_p =$

$15.2h^{-1}$  kpc and a relative velocity of  $\Delta v \sim 130$  km  $s^{-1}$ . The line targeted in this case is [O III] $\lambda$ 5007, which explains the low signal. The companion galaxy is toward the south-east, while the luminosity differences are  $\Delta m_i = 0.2$  and  $\Delta m_{K_s} = 0.1$ . We classify the system as a major merger.

- 020218856 (Fig. 11). **No major merger.** A faint companion is detected in the velocity map about  $1.6$  arcsec from the principal galaxy. There is no continuum detection of this companion at the depth of the  $i$ -band image. We followed the same steps than for the source 140096645 to estimate the detection probability of companion galaxies, finding that we are

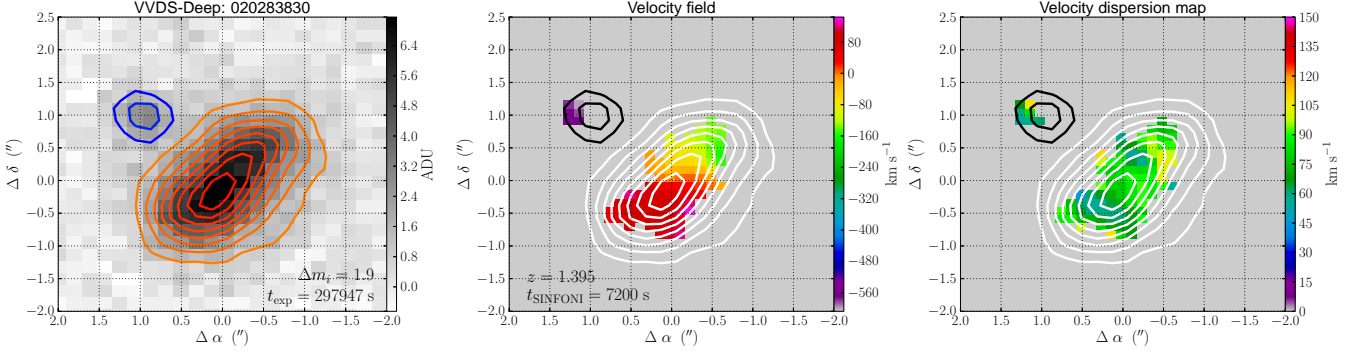


**Fig. 14.** The same as Fig. 3, but for the MASSIV source 020283830 (no major merger). The outer contour marks the 1.14 ADU ( $3.5\sigma_{\text{sky}}$ ) isophote, while brighter isophotes increase in 0.75 ADU ( $2.3\sigma_{\text{sky}}$ ) steps. [A colour version of this plot is available at the electronic edition].

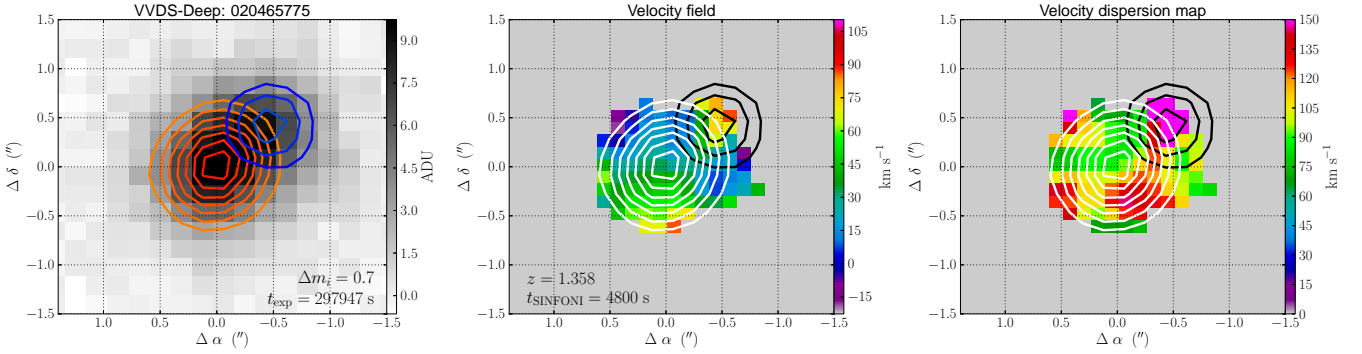


**Fig. 15.** The same as Fig. 3, but for the MASSIV source 020465775 (major merger). The outer contour marks the 2.92 ADU ( $9\sigma_{\text{sky}}$ ) isophote, while brighter isophotes increase in 0.97 ADU ( $3\sigma_{\text{sky}}$ ) steps. [A colour version of this plot is available at the electronic edition].

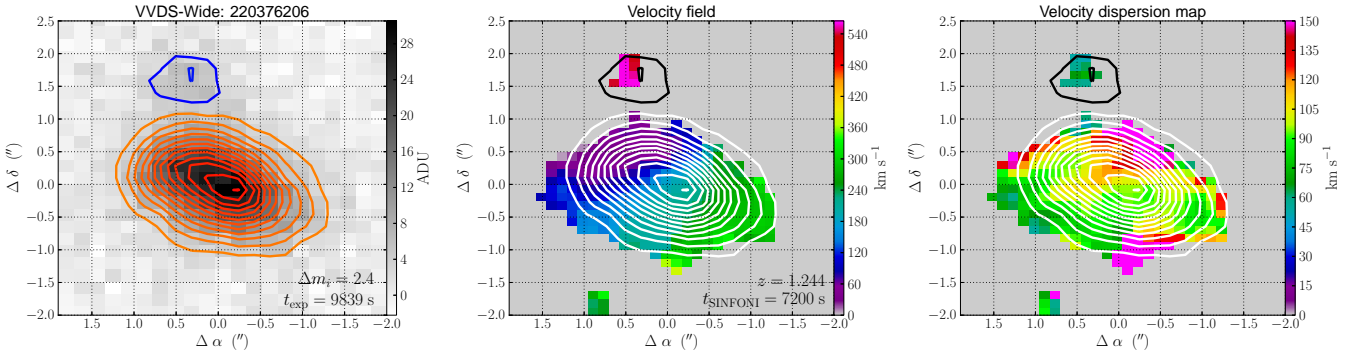


**Fig. 16.** The same as Fig. 3, but for the MASSIV source 220376206 (no major merger). The outer contour marks the 3.39 ADU ( $3\sigma_{\text{sky}}$ ) isophote, while brighter isophotes increase in 2.26 ADU ( $2\sigma_{\text{sky}}$ ) steps. [A colour version of this plot is available at the electronic edition].

100% complete up to  $m_{i,2} = 26$ . We note that the curves for extended, normal and compact galaxies are similar, reflecting that the size of the PSF is larger than the assumed size of the fake sources. Because a major companion should be brighter than  $m_{i,2}^{\text{MM}} = 25.32$  (vertical line in the left panel of Fig. 11), and the non detection in the continuum means that the companion should have  $\Delta m_i \gtrsim 2$ , we do not classify the system as a major merger.

- 020240675 (Fig. 12). *No major merger.* A faint companion is detected in the velocity map about 2.4 arcsec from the principal galaxy. There is no continuum detection of this compan-

ion at the depth of the  $i$ -band image. We followed the same steps than for the source 020218856 to estimate the detection curves of companion galaxies. We find similar completeness curves. Because a major companion should be brighter than  $m_{i,2}^{\text{MM}} = 25.15$  (vertical line in the left panel of Fig. 12), and the non detection in the continuum means that the companion should have  $\Delta m_i \gtrsim 2.5$ , we do not classify the system as a major merger.

- 020283083 (Fig. 13). **Major merger.** The velocity map suggests two projected components separated by  $3.8h^{-1}$  kpc and  $\sim 5 \text{ km s}^{-1}$ , with an extended region in the north-west. The

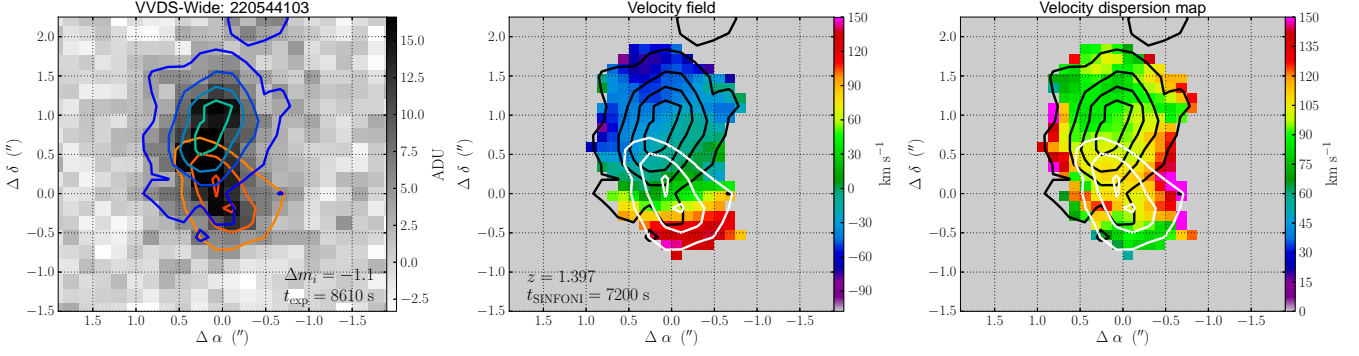


**Fig. 17.** The same as Fig. 3, but for the MASSIV source 220544103 (major merger). The outer contour marks the 3.32 ADU ( $2\sigma_{\text{sky}}$ ) isophote, while brighter isophotes increase in 3.32 ADU ( $2\sigma_{\text{sky}}$ ) steps. [A colour version of this plot is available at the electronic edition].

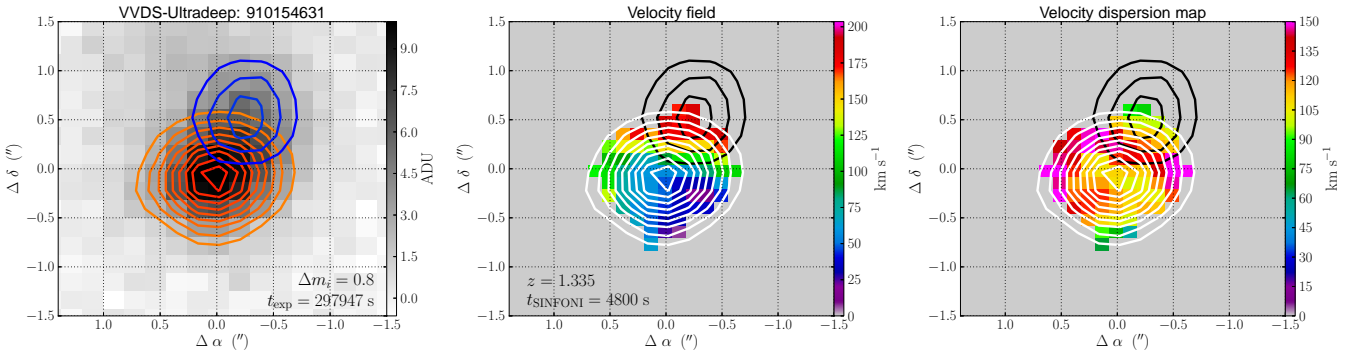


**Fig. 18.** The same as Fig. 3, but for the MASSIV source 910154631 (major merger). The outer contour marks the 1.9 ADU ( $6\sigma_{\text{sky}}$ ) isophote, while brighter isophotes increase in 0.8 ADU ( $2.5\sigma_{\text{sky}}$ ) steps. [A colour version of this plot is available at the electronic edition].

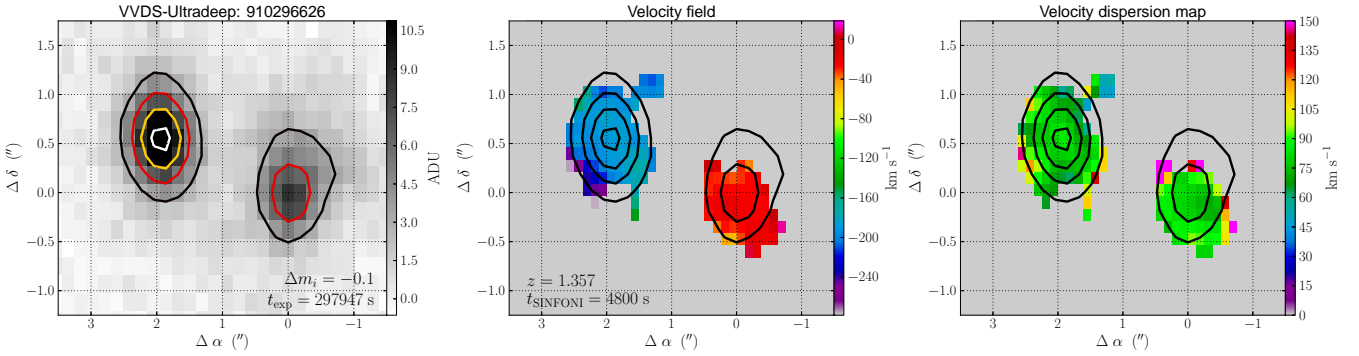


**Fig. 19.** The same as Fig. 8, but for the MASSIV source 910296626 (major merger). The outer contour marks the 3.32 ADU ( $10\sigma_{\text{sky}}$ ) isophote, while brighter isophotes increase in 2.56 ADU ( $8\sigma_{\text{sky}}$ ) steps. [A colour version of this plot is available at the electronic edition].

GALFIT model with two components reproduces the shape of the velocity map and suggests that the extended region is due to the companion galaxy. The luminosity difference from the models is  $\Delta m_i = 0.7$ . Thus, we classify this system as a major merger.

- 020283830 (Fig. 14). *No major merger.* The velocity map shows two different components with a separation of  $r_p = 8.5h^{-1}$  kpc and a relative velocity of  $\Delta v \sim 500$  km s $^{-1}$ . The companion only presents six detected pixels in the H $\alpha$  map, already suggesting a minor companion. We used GALFIT to model the system, finding  $\Delta m_i = 1.9$ . However, the model of

the companion provided by GALFIT is a point-like source, thus overestimating the luminosity of the extended companion. The measurement with SExtractor in the image with the principal galaxy subtracted suggests  $\Delta m_i = 2.1$ . Since the companion is fainter than the major merger limit, we do not classify the system as a major merger.

- 020465775 (Fig. 15). **Major merger.** The velocity map suggests two projected components. The GALFIT model with two components finds that the companion galaxy is toward the north-west of the principal galaxy, at  $r_p = 3.6h^{-1}$  kpc and  $\Delta v \sim 40$  km s $^{-1}$ . The H $\alpha$  emission of this system is located



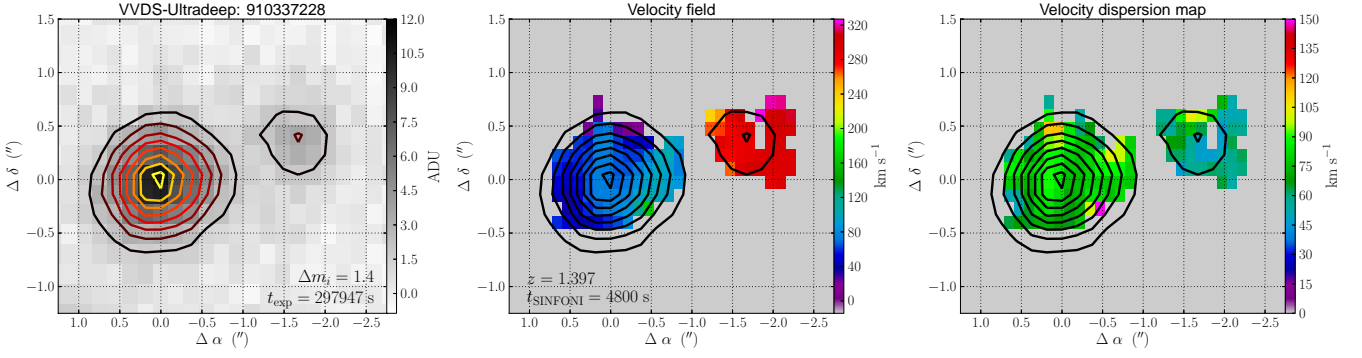


**Fig. 20.** The same as Fig. 8, but for the MASSIV source 910337228 (major merger). The outer contour marks the 1.73 ADU ( $4\sigma_{\text{sky}}$ ) isophote, while brighter isophotes increase in 1.30 ADU ( $3\sigma_{\text{sky}}$ ) steps. [A colour version of this plot is available at the electronic edition].

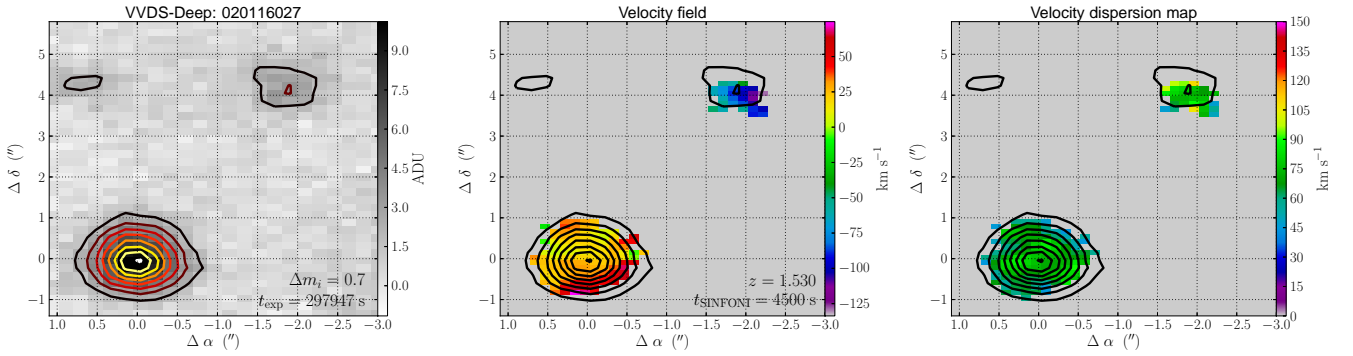


**Fig. 21.** The same as Fig. 8, but for the MASSIV source 020116027 (major merger). The principal galaxy is that in the south-east. The outer contour marks the 2.02 ADU ( $3.5\sigma_{\text{sky}}$ ) isophote, while brighter isophotes increase in 1.16 ADU ( $2\sigma_{\text{sky}}$ ) steps. [A colour version of this plot is available at the electronic edition].

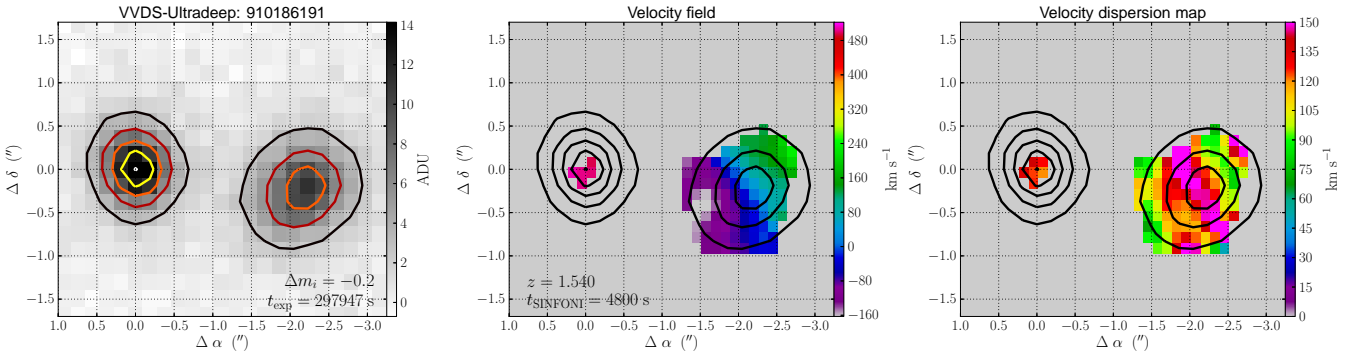


**Fig. 22.** The same as Fig. 3, but for the MASSIV source 910186191 (major merger). The outer contour marks the 2.83 ADU ( $8\sigma_{\text{sky}}$ ) isophote, while brighter isophotes increase in 2.83 ADU ( $8\sigma_{\text{sky}}$ ) steps. [A colour version of this plot is available at the electronic edition].

in the central part of the galaxies, since the  $i$ -band models match the velocity map at  $9\sigma_{\text{sky}}$  level, i.e., we do not detect emission from the outer parts of the galaxies. The position of the companion explains the abnormal velocity pattern and the high velocity dispersion peak in the maps. The luminosity difference of the system is  $\Delta m_i = 0.7$ , so we classify it as a major merger.

- 220376206 (Fig. 16). *No major merger.* The velocity map shows two different components with a separation of  $r_p = 13.4h^{-1}$  kpc and a relative velocity of  $\Delta v \sim 400$  km s $^{-1}$ . The companion, located toward the north, presents ten detected

pixels and its velocity is inconsistent with that expected from the velocity field of the principal galaxy. We find  $\Delta m_i = 2.4$ , so the system is not a major merger.

- 220544103 (Fig. 17). **Major merger.** The velocity map suggests two projected components. The southern component presents a large velocity gradient and defines the kinematical centre of the system, while the northern component is more extended and has a nearly flat velocity field. The GALFIT model with two components recovers the configuration in the velocity map and suggests that the southern component is edge-on, while the northern component is nearly face-on,



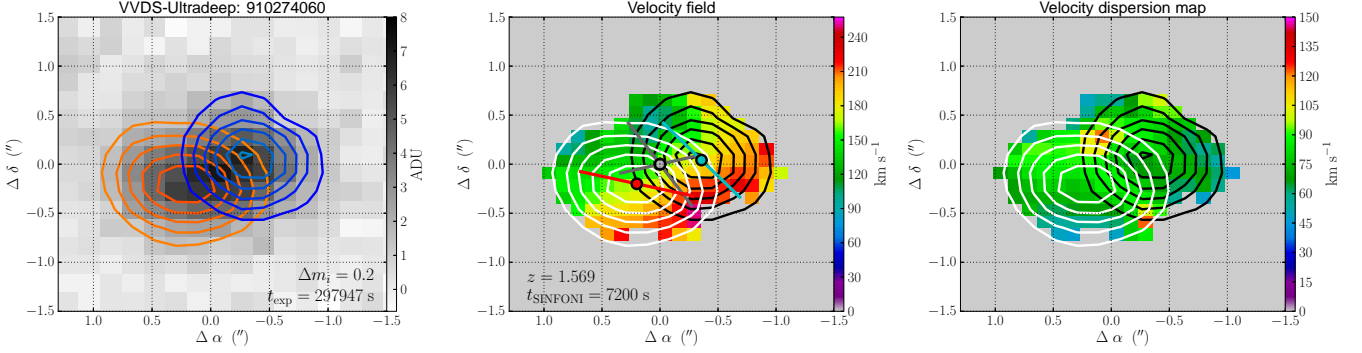


**Fig. 23.** The same as Fig. 3, but for the MASSIV source 910274060 (major merger). The outer contour marks the 1.20 ADU ( $3\sigma_{\text{sky}}$ ) isophote, while brighter isophotes increase in 1.00 ADU ( $2.5\sigma_{\text{sky}}$ ) steps. The grey dot in the central figure marks the centre of the system given by the kinematical model, while the red/blue dot marks the photometric centre of the principal/companion galaxy given by the two-component model of the source. The long bars mark the position angle of the previous models. The short bar marks the photometric position angle given by the one-component model of the source. [A colour version of this plot is available at the electronic edition].

thus explaining the observed high and null velocity gradients. The separation between the components is  $r_p = 5h^{-1}$  kpc, while their relative velocity is  $\Delta v \sim 75 \text{ km s}^{-1}$ . From the GALFIT models we estimate  $\Delta m_i = -1.1$ , and we classify the system as a major merger.

- 910154631 (Fig. 18). **Major merger.** The velocity map suggests two projected components, with the companion toward the north-west. The  $i$ -band image shows another two well separated sources close to the MASSIV target. These sources are not detected in  $H\alpha$ . To avoid contamination from these sources in the  $i$ -band photometry, we performed a four component fitting, with two components for the MASSIV target and one component for each nearby source. The GALFIT model finds the second component of the MASSIV target at the expected position, but we only detect the southern half of the  $i$ -band source in  $H\alpha$ . We explored the reduced data cube of the source, and we find (i) there are two clear velocity gradients in the cube, reinforcing the presence of two different components and (ii) there is an OH sky-line in the channels in which we expect the northern part of the companion, explaining the non detection in the maps. In addition, the higher velocity dispersion of the MASSIV target occurs in the expected overlapping region between both components. We conclude that this is a close pair system with  $r_p = 4.2h^{-1}$  kpc,  $\Delta v \sim 130 \text{ km s}^{-1}$  and  $\Delta m_i = 0.8$ . Thus, we classify the system as a major merger.
- 910296626 (Fig. 19). **Major merger.** The velocity map shows two different components with a separation of  $r_p = 12.1h^{-1}$  kpc and a relative velocity of  $\Delta v \sim 165 \text{ km s}^{-1}$ . The companion is located toward the north-east. We find  $\Delta m_i = -0.1$  and  $\Delta m_{K_s} = -0.2$ , so the system is a major merger.
- 910337228 (Fig. 20). **Major merger.** The velocity map shows two different components with a separation of  $r_p = 9.5h^{-1}$  kpc and a relative velocity of  $\Delta v \sim 220 \text{ km s}^{-1}$ . The companion is toward the west and has  $\Delta m_i = 1.4$ . Thus, we classify the system as a major merger.

In summary for this redshift range, we classify 7 of the 11 close pair candidates as major mergers. This translates to a gas-rich major merger fraction of  $f_{\text{MM}} = 0.201_{-0.051}^{+0.080}$  at  $\bar{z}_{r,2} = 1.32$ .

#### 4.3. Close pair candidates at $1.5 \leq z < 1.8$

The weighted mean redshift of the third redshift bin is  $\bar{z}_{r,3} = 1.54$ . This is a redshift range where there is no measurement of the merger fraction from spectroscopic close pairs yet. We identify 3 close pair candidates over 12 galaxies:

- 020116027 (Fig. 21). **Major merger.** The velocity map shows two different components with a separation of  $r_p = 26.8h^{-1}$  kpc and a relative velocity of  $\Delta v \sim 100 \text{ km s}^{-1}$ . The companion is toward the north-west. The luminosity difference is  $\Delta m_i = 0.7$ , suggesting a major merger. The difference in the  $K_s$  band is  $\Delta m_{K_s} = 0.5$ , confirming the previous major merger classification.
- 910186191 (Fig. 22). **Major merger.** The velocity map shows two different components with a separation of  $r_p = 12.7h^{-1}$  kpc and a relative velocity of  $\Delta v \sim 450 \text{ km s}^{-1}$ . The MASSIV target is only detected in 6 pixels because there is an OH sky-line in the position of  $H\alpha$  at its redshift. The companion, located toward the west, is well detected. We find  $\Delta m_i = -0.2$ , this is, the companion is slightly brighter than the principal galaxy. However, the MASSIV target is barely detected in the  $K_s$  band, with  $\Delta m_{K_s} = -2.4$ , suggesting a low mass system. This is the only system in which the classification in the two bands is different. Fortunately, both sources are VVDS targets, and we have an estimation of their stellar masses from SED fitting. The difference in stellar mass is  $\mu \sim 1/3$ , so we classify the system as a major merger.
- 910274060 (Fig. 23). **Major merger.** The velocity map is consistent with one single component. However, the position angle (PA) from the  $i$ -band photometry,  $\text{PA} = 105^\circ$  (North has  $\text{PA} = 0^\circ$  and East has  $\text{PA} = 90^\circ$ ), is nearly perpendicular to that from the kinematical modelling,  $\text{PA} = 33^\circ$ . This suggests a complex system, so we performed the GALFIT modelling with two sources. We recover well two sources, one in the north and the other in the south. The photometric PAs of these two sources, provided by the GALFIT fitting, are now in better agreement with the kinematical one ( $\text{PA}_1 = 75^\circ$ ,  $\text{PA}_2 = 41^\circ$ ), supporting that this is a close pair system. The separation between the components is  $3.4h^{-1}$  kpc, with  $\Delta v \sim 10 \text{ km s}^{-1}$ , and the luminosity difference is  $\Delta m_i = 0.2$ . Thus, we classify the system as a major merger.

In summary, we identify the 3 candidates as major mergers. This translates to a gas-rich major merger fraction of  $f_{\text{MM}} = 0.323^{+0.201}_{-0.107}$ . Note that in this range our merger candidates have  $r_{\text{p}}^{\text{max}} = 30h^{-1}$  kpc to improve the statistics. Applying Eq. (7) we estimate  $f_{\text{MM}} = 0.220^{+0.137}_{-0.073}$  for  $r_{\text{p}}^{\text{max}} = 20h^{-1}$  kpc at  $\bar{z}_{r,3} = 1.54$ .

Our results alone, summarised in Table 2, suggest a constant major merger fraction of  $f_{\text{MM}} \sim 0.21$  at  $0.9 < z < 1.8$  for  $r_{\text{p}}^{\text{max}} = 20h^{-1}$  kpc close pairs (Fig. 24). *This merger fraction at  $z > 1$  is higher by an order of magnitude than in the local universe, where  $f_{\text{MM}} \sim 0.01 - 0.03$  (Patton et al. 2000; De Propris et al. 2007; Patton & Atfield 2008; Domingue et al. 2009; Darg et al. 2010; Xu et al. 2012).* This is the first main result of the present paper. We compare our major merger fractions with others in the literature in Sect. 6.1.

## 5. The gas-rich major merger rate in MASSIV

In this section we estimate the gas-rich major merger rate ( $R_{\text{MM}}$ ), defined as the number of mergers per galaxy and Gyr, of star-forming galaxies at  $0.9 < z < 1.8$ . We remind here the steps to transform a merger fraction to a merger rate. Following de Ravel et al. (2009), we define the major merger rate as

$$R_{\text{MM}} = C_{\text{m}} f_{\text{MM}} T_{\text{MM}}^{-1}, \quad (6)$$

where the factor  $C_{\text{m}}$  is the fraction of the observed close pairs that finally merge in a typical time scale  $T_{\text{MM}}$ . The typical merger time scale can be estimated by cosmological and  $N$ -body simulations. In our case, we compute the major merger time scale from the cosmological simulations of Kitzbichler & White (2008), based on the Millennium simulation (Springel et al. 2005). This major merger time scale refers to major mergers ( $\mu \geq 1/4$  in stellar mass), and depends mainly on  $r_{\text{p}}^{\text{max}}$  and on the stellar mass of the principal galaxy, with a weak dependence on redshift in our range of interest (see de Ravel et al. 2009, for details). We measured the median-weighted stellar mass from MASSIV sources in each of the three redshift bins under study, and estimated the merger time scale for these stellar masses. These time scales already include the factor  $C_{\text{m}}$  (see Patton & Atfield 2008; Bundy et al. 2009; Lin et al. 2010; López-Sanjuan et al. 2011), so we take  $C_{\text{m}} = 1$  in the following. In addition, López-Sanjuan et al. (2011) show that the time scales from Kitzbichler & White (2008) are equivalent to that from the  $N$ -body/hydrodynamical simulations by Lotz et al. (2008). However, we stress that these merger time scales have an additional factor of two uncertainty in their normalization (e.g., Hopkins et al. 2010; Lotz et al. 2011). We summarise the stellar masses, the merger time scales and the gas-rich major merger rates in Table 2. As for the merger fraction, MASSIV data suggests a nearly constant major merger rate at  $0.9 < z < 1.8$ ,  $R_{\text{MM}} \sim 0.12 \text{ Gyr}^{-1}$  (Fig. 25). We study in detail the evolution of the major merger rate at  $z \lesssim 1.5$  in Sect. 6.2.

## 6. The redshift evolution of the gas-rich major merger fraction and rate up to $z \sim 1.5$

In this section we use the MASSIV results at  $z > 1$  to expand the study of the gas-rich major merger fraction (Sect. 6.1) and rate (Sect. 6.2) from spectroscopic close pairs to the redshift desert. Then, we explore the importance of gas-rich major mergers in the assembly of the red sequence since  $z \sim 1.5$  in Sects. 6.3 and 6.4.

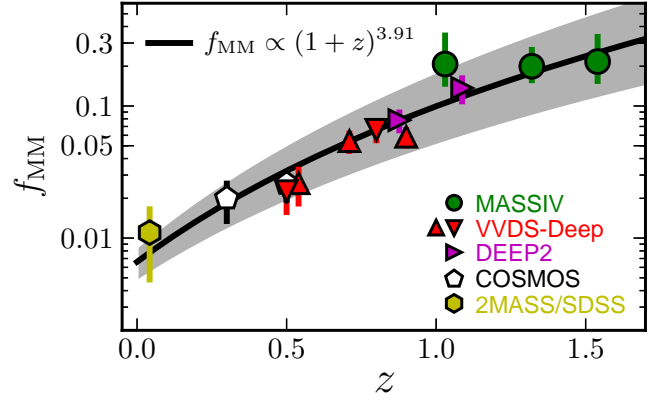


**Fig. 24.** Gas-rich major merger fraction of  $\bar{M}_{\star} \sim 10^{10-10.5} M_{\odot}$  galaxies as a function of redshift. Circles are from this MASSIV data set, triangles are from de Ravel et al. (2009) and inverted triangles are from López-Sanjuan et al. (2011), both in VVDS-Deep, right-pointing triangles are from Lin et al. (2008) in DEEP2 redshift survey, pentagons are from Xu et al. (2012) in the COSMOS field, and the hexagon is from Xu et al. (2012) in 2MASS/SDSS. The solid line is the least-squares fit of a power-law function,  $f_{\text{MM}} = 0.0066 \times (1+z)^{3.91}$ , to the data. The grey area marks the  $3\sigma$  confidence interval in the fit. [A colour version of this plot is available at the electronic edition].

### 6.1. The redshift evolution of the gas-rich major merger fraction

In this section we compare the merger fraction from MASSIV with those from previous works. Because the merger fraction evolution depends on mass (e.g., de Ravel et al. 2009, 2011), luminosity (e.g., de Ravel et al. 2009; López-Sanjuan et al. 2010a) and colour (e.g., Lin et al. 2008; Chou et al. 2011), we focus on samples with  $\bar{M}_{\star} \sim 10^{10-10.5} M_{\odot}$  (Salpeter 1955 IMF) to minimise systematics. In addition, this mass regime is greatly dominated by gas-rich (wet) mergers, as those that we observe in MASSIV, at least at  $z \gtrsim 0.2$  (Lin et al. 2008; de Ravel et al. 2009; Chou et al. 2011).

We define the major ( $\mu \geq 1/4$ ) merger fraction normalised to  $r_{\text{p}}^{\text{max}} = 20h^{-1}$  kpc as

$$f_{\text{MM}}(20, 1/4) = C_{\text{p}} F(\mu) \left( \frac{20h^{-1} \text{ kpc}}{r_{\text{p}}^{\text{max}}} \right)^{0.95} f_{\text{m}}(r_{\text{p}}^{\text{max}}, \mu), \quad (7)$$

where the factor  $C_{\text{p}} = r_{\text{p}}^{\text{max}} / (r_{\text{p}}^{\text{max}} - r_{\text{p}}^{\text{min}})$  accounts for the missing close companions at small radii in those studies with  $r_{\text{p}}^{\text{min}} > 0$  (e.g., Bell et al. 2006) and the factor  $F(\mu)$  translates the merger fraction for a given  $\mu$  to the major merger fraction. The merger fraction depends on  $\mu$  as  $f_{\text{m}}(\geq \mu) \propto \mu^s$  (e.g., López-Sanjuan et al. 2011), that implies  $F(\mu) = (4\mu)^{-s}$ . We take  $s = -0.9 \pm 0.4$ , a value derived from the observational estimations of López-Sanjuan et al. (2011, 2012) and Xu et al. (2012). The search radius dependence of the major merger fraction,  $f_{\text{MM}} \propto r_{\text{p}}^{0.95}$ , is the observational one found by López-Sanjuan et al. (2011) in the VVDS. With Eq. (7) we avoid systematic differences due to the close pair definition when comparing different works.

de Ravel et al. (2009) study the major merger fraction of  $M_{\star} \geq 10^{9.75} M_{\odot}$  ( $\bar{M}_{\star} \sim 10^{10.25} M_{\odot}$ ) galaxies in VVDS-Deep by spectroscopic close pairs, while López-Sanjuan et al. (2011) provide the major merger fraction of blue (star-forming)

**Table 2.** Gas-rich major merger fraction and rate of star-forming galaxies at  $0.9 < z < 1.8$  in the MASSIV sample.

$z_r$	$N$	$N_p$	$\bar{z}_r$	$\log(\bar{M}_*/M_\odot)$	$r_p^{\max}$ ( $h^{-1}$ kpc)	$T_{MM}$ (Gyr)	$f_{MM}$	$R_{MM}$ ( $\text{Gyr}^{-1}$ )
$0.94 \leq z \leq 1.06$	18	3	1.03	10.17	20	1.80	$0.208^{+0.152}_{-0.068}$	$0.116^{+0.084}_{-0.038}$
$1.2 \leq z < 1.5$	30	7	1.32	10.57	20	1.37	$0.201^{+0.080}_{-0.051}$	$0.147^{+0.058}_{-0.037}$
$1.5 \leq z < 1.8$	12	3	1.54	10.09	30	2.54	$0.323^{+0.201}_{-0.107}$	$0.127^{+0.079}_{-0.042}$

galaxies with  $\bar{M}_* \sim 10^{10.55} M_\odot$  in the same sample. In both studies  $r_p^{\max} = 100h^{-1}$  kpc. Lin et al. (2008) report the number of companions of  $-21 \leq M_B + 1.3z \leq -19$  galaxies ( $\bar{M}_* \sim 10^{10.25} M_\odot$ ) with  $10h^{-1}$  kpc  $\leq r_p \leq 30h^{-1}$  kpc in three DEEP2 redshift survey (Newman et al. 2012b) fields. Their principal and companion sample are the same, so they miss major companions near to the selection boundary. Thus, we apply an extra factor 1.74 to Eq. (7) to account for these missing companions (see Lin et al. 2004, for details). Xu et al. (2012) measure the fraction of galaxies in close pairs with  $\mu \geq 1/2.5$  in the COSMOS<sup>4</sup> (Cosmological Evolution Survey, Scoville et al. 2007) and SDSS<sup>5</sup> (Sloan Digital Sky Survey, Abazajian et al. 2009) surveys for  $\bar{M}_* \sim 10^{10.2} M_\odot$  galaxies. We applied a factor 0.5 to pass from their number of galaxies in close pairs to the number of close pair systems in the sample (C. K. Xu, private communication), and a factor  $F(1/2.5) = 1.5 \pm 0.3$  to obtain the major merger fraction. All these published (gas-rich) major merger fractions are shown as a function of redshift in Fig. (24), together with the values derived from MASSIV.

We parametrise the redshift evolution of the (gas-rich) major merger fraction with a power-law,

$$f_{MM} = f_{MM,0} (1+z)^m. \quad (8)$$

The least-squares fit to all the data in Fig. 24 yields  $f_{MM,0} = (6.6 \pm 0.6) \times 10^{-3}$  and  $m = 3.91 \pm 0.16$ . We find good agreement between all works, with the MASSIV point at  $z \sim 1$  being higher than expected from the fit, but consistent within errors with the measurement of Lin et al. (2008) at that redshift. In the next section we show that this difference disappears when the stellar mass of the samples is taken into account, emphasizing the importance of comparing results from similar parent samples.

## 6.2. The redshift evolution of the gas-rich major merger rate

We use Eq. (6) to translate the original (i.e., without any normalization in  $r_p^{\max}$ ) major merger fractions reported in previous section into merger rates. We show them in Fig. 25. The good agreement between different works is remarkable, reinforcing the idea that the merger time scales used account properly for the dependence of the merger fraction both on  $r_p^{\max}$  and on stellar mass.

We also show the major merger rate from morphological criteria derived by López-Sanjuan et al. (2009b). They measure the gas-rich merger fraction of  $\bar{M}_* \sim 10^{10.5} M_\odot$  galaxies from asymmetries ( $A$ ) in the GOODS<sup>6</sup> (Giavalisco et al. 2004) South field and take into account the effect of observational

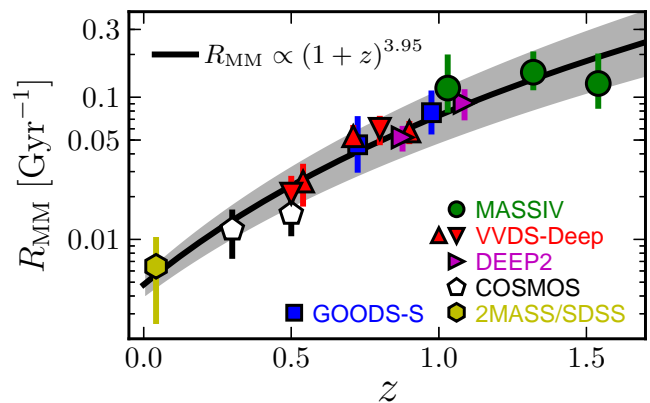


**Fig. 25.** Gas-rich major merger rate of  $\bar{M}_* \sim 10^{10-10.5} M_\odot$  galaxies as a function of redshift. Circles are from this MASSIV data set, triangles are from de Ravel et al. (2009) and inverted triangles are from López-Sanjuan et al. (2011), both in VVDS-Deep, right-pointing triangles are from Lin et al. (2008) in DEEP2 redshift survey, squares are from López-Sanjuan et al. (2009b) in GOODS-S from morphological criteria, pentagons are from Xu et al. (2012) in the COSMOS field, and the hexagon is from Xu et al. (2012) in 2MASS/SDSS. The solid line is the least-squares fit of a power-law function,  $R_{MM} = 0.0048 \times (1+z)^{3.95}$ , to the data. The grey area marks the  $3\sigma$  confidence interval in the fit. [A colour version of this plot is available at the electronic edition].

errors in  $z$  and  $A$ , that lead to overestimations in the major merger fraction by a factor of two-three (López-Sanjuan et al. 2009a,b), using maximum likelihood techniques developed in López-Sanjuan et al. (2008). Other studies find good agreement between the asymmetry-based major merger rates from López-Sanjuan et al. (2009b) and those from close pair statistics (López-Sanjuan et al. 2010a; Lotz et al. 2011; de Ravel et al. 2011), confirming the robustness of their methodology.

We also parametrise the redshift evolution of the (gas-rich) major merger rate with a power-law,

$$R_{MM} = R_{MM,0} (1+z)^n. \quad (9)$$

The least-squares fit to all the data in Fig. 25 yields  $R_{MM,0} = (4.8 \pm 0.3) \times 10^{-3} \text{ Gyr}^{-1}$  and  $n = 3.95 \pm 0.12$ . The agreement between different works points out the importance of comparing results from similar parent samples to avoid systematics (see also Lotz et al. 2011, for an extensive discussion on this topic). We also point out that the merger rate and the merger fraction of star-forming galaxies show a similar evolution with redshift.

The second main result in this paper is that *the major merger rate is well described by a power-law function up to*

<sup>4</sup> <http://cosmos.astro.caltech.edu>

<sup>5</sup> <http://www.sdss.org/>

<sup>6</sup> <http://www.stsci.edu/science/goods/>

$z \sim 1.5$ . However, we note that our MASSIV data seem to indicate a flattening of the merger rate's evolution beyond  $z \sim 1$ . Previous studies from morphological criteria (e.g., Conselice 2003; Conselice et al. 2008) and from photometric pairs (Ryan et al. 2008) suggest that the power-law parametrization is not longer valid at  $z \gtrsim 1.5$ , where a lower merger fraction than expected from the low- $z$  evolution is measured, possibly indicating a maximum in the major merger rate at  $z \sim 2$  (e.g., Conselice 2006; Ryan et al. 2008; López-Sanjuan et al. 2009b). Our new measurements agree with this picture and measurements from spectroscopic close pairs beyond  $z \sim 1.5$  are needed to test the early evolution of the merger fraction.

The power-law index  $n = 3.95 \pm 0.12$  is higher than several previous measurements in the literature (e.g., Bridge et al. 2010; Lotz et al. 2011), as well as our major merger fraction evolution,  $m = 3.91 \pm 0.16$ . However, our results refer to  $\bar{M}_* \sim 10^{10-10.5} M_\odot$  star-forming galaxies, and it is known that the merger fraction and rate evolve faster for blue, star-forming galaxies than for the red and global populations (e.g., Lin et al. 2008; de Ravel et al. 2009; Chou et al. 2011; López-Sanjuan et al. 2011).

### 6.3. Number of gas-rich mergers since $z = 1.5$

We can obtain the average number of gas-rich major mergers per star-forming galaxy between  $z_2$  and  $z_1 < z_2$  as

$$N_{\text{MM}}(z_1, z_2) = \int_{z_1}^{z_2} \frac{R_{\text{MM}} dz}{(1+z)H_0 E(z)}, \quad (10)$$

where  $E(z) = \sqrt{\Omega_\Lambda + \Omega_m(1+z)^3}$  in a flat universe. Using the merger rate parametrisation in Eq. (9), we obtain  $N_{\text{MM}}(0, 1.5) = 0.35 \pm 0.04$ . Interestingly, half of this merging activity happens at  $z > 1$ , with  $N_{\text{MM}}(1, 1.5) = 0.18 \pm 0.02$  and  $N_{\text{MM}}(0, 1) = 0.17 \pm 0.02$ . Because the cosmic time lapse in these redshift intervals is 1.55 Gyr and 7.7 Gyr, respectively, the average merger activity was higher at  $1 < z < 1.5$  than at  $1 < z$  by a factor of five. In the next section we further explore the consequences of this very different major merger activity above and below  $z \sim 1$  for the assembly of the red sequence.

### 6.4. Testing the major merger origin of massive early-type galaxies

The number density of massive ( $M_* \gtrsim 10^{11} M_\odot$ ) early-type galaxies (E/S0, ETGs in the following) has increased with cosmic time since  $z \sim 3$  (e.g., Pozzetti et al. 2010; Buitrago et al. 2013), with ETGs being the dominant population among massive galaxies only since  $z \sim 1$  (Vergani et al. 2008; Buitrago et al. 2013; van der Wel et al. 2011; van Dokkum et al. 2011). Gas-rich major mergers have been proposed as an efficient mechanism to transform star-forming late-type galaxies into red ETGs (e.g., Naab et al. 2006; Rothberg & Joseph 2006a,b; Hopkins et al. 2008; Rothberg & Fischer 2010; Bournaud et al. 2011), so the comparison between the observed number density evolution of ETGs ( $\rho_{\text{ETG}}$ ) and the major merger history of star-forming galaxies imposes important constraints on the role of mergers in galaxy evolution.

In their work, Robaina et al. (2010) and Man et al. (2012) integrate the observed major merger rate over cosmic time and predict the evolution of the number density of massive galaxies assuming that all the merger remnants are new massive galaxies. They suggest that major mergers are common enough to explain the number density evolution of massive galaxies (ETGs

+ spirals) at  $z < 1$  and  $z < 3$ , respectively. Eliche-Moral et al. (2010) model the evolution of the luminosity function backwards in time for bright galaxies, selected according to their colours (red/blue/total) and their morphologies. They find that the observed luminosity functions' evolution can be naturally explained by the observed gas-rich and dry major merger rates, and that 50-60% of massive ETGs in the local universe were formed by major mergers at  $0.8 < z < 1$ , with a small number evolution since  $z = 0.8$ .

In this section we implement a model to explore the role of mergers in the number density evolution of massive ETGs since  $z \sim 1.3$ . As reference values, we use the number densities of massive ( $M_* \geq 10^{11.25} M_\odot$ ) ETGs provided by Buitrago et al. (2013). They perform a consistent morphological study by visual inspection between  $z = 0$  and  $z = 3$ , combining the SDSS, POWIR (Palomar Observatory Wide-Field Infrared, Conselice et al. 2007) and GNS<sup>7</sup> (GOODS NICMOS Survey, Conselice et al. 2011a) surveys. We also use the number densities of massive spheroidal galaxies with  $M_* \geq 10^{11.25} M_\odot$ , selected by automatic indices in the zCOSMOS<sup>8</sup> (Lilly et al. 2007) survey, provided by Pozzetti et al. (2010). We show these number densities in Fig. 26.

In our model we assume that, after the final coalescence of the merging galaxies, a cosmic time  $\Delta t = 0.5$  Gyr is necessary for the merger remnant to be classified as an ETG (see Eliche-Moral et al. 2010, for a detailed summary of this topic). This implies that the new ETGs which appeared between  $z_{\text{max}}$  and  $z_{\text{min}}$  came from the merger activity in the range  $z \in [z_1, z_2]$ , where  $z_1 = z_{\text{min}} + \Delta z$ ,  $z_2 = z_{\text{max}} + \Delta z$ , and  $\Delta z$  is the redshift interval that spans  $\Delta t$  in each case. Therefore, we take  $z_{\text{max}} = 1.3$  as the upper redshift in our model because that implies  $z_2 \sim 1.5$ , the redshift limit of the present merger rate study (see Sect. 6.2).

The number density of new ETGs with stellar mass  $M_* \geq M_{*,\text{lim}}$  from gas-rich major merger events appeared in the range  $z_{\text{min}} \leq z < z_{\text{max}}$  is

$$\rho_{\text{wet}}(z_{\text{min}}, z_{\text{max}}, M_{*,\text{lim}}) = \int_{z_1}^{z_2} \int_0^\infty \Phi R_{\text{MM}} E_{\text{MM}} f_{\text{LTG}} dM_* dz, \quad (11)$$

where the different elements in the integral are (Fig. 27):

- the global mass function, parametrised with a Schechter function

$$\Phi(z, M_*) = \frac{\phi^*(z)}{M_*^*(z)} \left( \frac{M_*}{M_*^*(z)} \right)^{\alpha(z)} \exp\left( - \frac{M_*}{M_*^*(z)} \right). \quad (12)$$

We assumed the Schechter function parameters from Pérez-González et al. (2008) and used their parametrisation with redshift provided by López-Sanjuan et al. (2010a),

$$\log(\phi^*(z)/\text{Mpc}^{-3}) = -2.72 - 0.56(z - 0.5), \quad (13)$$

$$\log(M_*^*(z)/M_\odot) = 11.23 + 0.13(z - 0.5), \quad (14)$$

$$\alpha(z) = -1.22 - 0.04(z - 0.5). \quad (15)$$

- The gas-rich major merger rate,  $R_{\text{MM}}(z)$ , as measured in Sect. 6.2. We assumed that it is independent of the stellar mass.
- The merger efficiency function,  $E(z, M_*, M_{*,\text{lim}}, \mu_{\text{max}}, \mu_{\text{min}})$ . This function provides the probability that a gas-rich merger with a mass ratio  $\mu_{\text{min}} < \mu \leq \mu_{\text{max}}$  produces an early-type remnant more massive than  $M_{*,\text{lim}}$ . The merger efficiency function takes several effects into account:

<sup>7</sup> <http://www.nottingham.ac.uk/astronomy/gns/>

<sup>8</sup> <http://www.astro.phys.ethz.ch/zCOSMOS/>



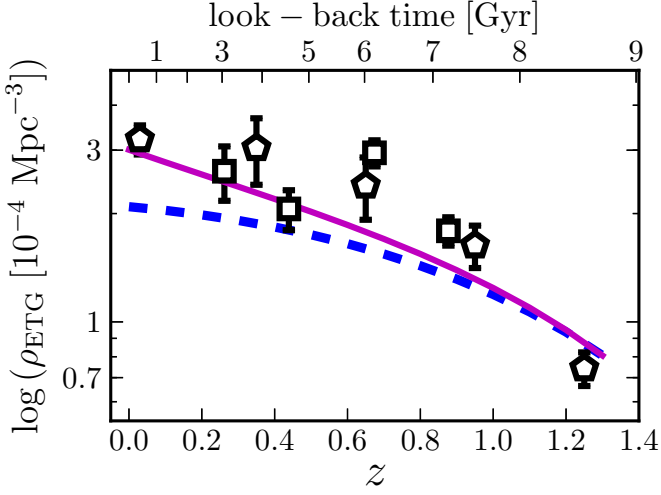


**Fig. 26.** Number density evolution of massive ( $M_{\star} \geq 10^{11.25} M_{\odot}$ ) ETGs (E/S0) as a function of redshift from Buitrago et al. (2013, pentagons) and Pozzetti et al. (2010, squares). The dashed line is the expected number density evolution due to gas-rich (wet) major mergers from our model. The solid line is the expected number density evolution due to wet major and dry mergers (both major and minor) from our model. Mergers are common enough to drive the number density evolution of massive ETGs since  $z \sim 1.3$ . [A colour version of this plot is available at the electronic edition].

- The stellar mass difference  $\mu$  needed to reach  $M_{\star, \text{lim}}$  for a given  $M_{\star}$ . For example, and regarding major mergers with  $\mu \geq 1/4$ , the  $\mu_{\text{max}} = 1$  mergers of galaxies with  $M_{\star} \geq 10^{10.7} M_{\odot}$  will provide a massive remnant with  $M_{\star} \geq M_{\star, \text{lim}} = 10^{11} M_{\odot}$ , while for  $\mu_{\text{min}} = 1/4$  only galaxies with  $M_{\star} \geq 10^{10.9} M_{\odot}$  can be progenitors of massive ETGs. Thus, mergers below  $M_{\star, \text{lim}}/(1 + \mu_{\text{min}})$  do not contribute to the assembly of massive ETG, while all mergers above  $M_{\star, \text{lim}}/(1 + \mu_{\text{max}})$  contribute. Between  $\mu_{\text{min}}$  and  $\mu_{\text{max}}$ , we used the dependence of the merger fraction on the mass ratio  $\mu$ ,  $f_{\text{MM}} \propto \mu^s$  (e.g., López-Sanjuan et al. 2011), to estimate the effective merger rate at  $M_{\star} = M_{\star, \text{lim}}/(1 + \mu)$ .
- The extra stellar mass in the final remnant due to the star formation during the merger,  $f_{\text{sf}}$ . This extra stellar mass simply decreases the limiting mass for a given  $\mu$  described in the previous item by a factor  $(1 + f_{\text{sf}})^{-1}$ .
- The fraction of remnants of a gas-rich major merger that are ETGs. We express this fraction as  $1 - f_{\text{disc}}$ , where  $f_{\text{disc}}$  is the fraction of remnants that rebuild a disc component and are classified as late-type galaxies after the merger (see Sect. 6.4.2, for further details).

Formally, the merger efficiency function is defined as

$$E = \begin{cases} 1 - f_{\text{disc}}, & \text{if } M_{\star} \geq M_{\star, 1}, \\ (1 - f_{\text{disc}}) \times (\mu/\mu_{\text{min}})^s, & \text{if } M_{\star, 2} \leq M_{\star} < M_{\star, 1}, \\ 0, & \text{if } M_{\star} < M_{\star, 2}, \end{cases} \quad (16)$$

where

$$M_{\star, 1} = \frac{M_{\star, \text{lim}}}{(1 + \mu_{\text{min}})(1 + f_{\text{sf}})}, \quad (17)$$

$$M_{\star, 2} = \frac{M_{\star, \text{lim}}}{(1 + \mu_{\text{max}})(1 + f_{\text{sf}})}, \quad (18)$$

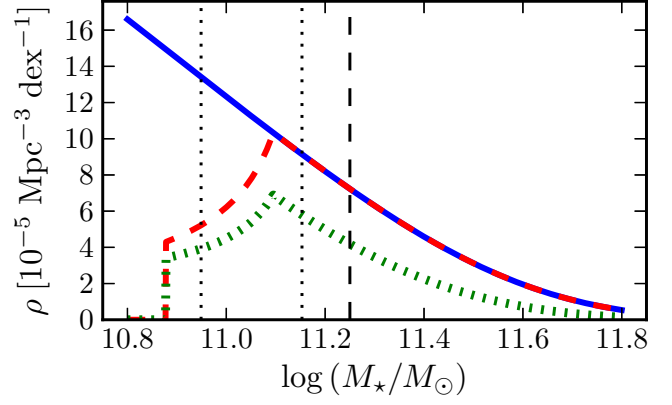


**Fig. 27.** Number density distribution from the different functions in Eq. (11) at  $z = 1$ . The solid line is the stellar mass function ( $\Phi$ ) multiplied by the major merger rate ( $R_{\text{MM}}$ ). The dashed line includes the major merger efficiency function ( $E_{\text{MM}}$ ). The dotted line includes the fraction of late-type galaxies ( $f_{\text{LTG}}$ ) and provides the final function that we integrate over stellar mass and cosmic time to obtain  $\rho_{\text{wet}}$ . The vertical dashed line marks the limiting stellar mass that define massive galaxies,  $M_{\star, \text{lim}} = 10^{11.25} M_{\odot}$ , while the dotted lines mark the stellar masses  $M_{\star, 1} = 10^{10.15} M_{\odot}$  and  $M_{\star, 2} = 10^{11.05} M_{\odot}$  when  $f_{\text{sf}} = 0$  (see text for details). [A colour version of this plot is available at the electronic edition].

$$\mu = \frac{M_{\star, \text{lim}}}{M_{\star}(1 + f_{\text{sf}})} - 1. \quad (19)$$

For convenience, we define the major merger efficiency in Eq. (11) as  $E_{\text{MM}} \equiv E(z, M_{\star}, M_{\star, \text{lim}}, \mu_{\text{max}} = 1, \mu_{\text{min}} = 1/4)$ . We assumed that  $f_{\text{disc}} = 0$ , i.e., all the merger remnants are ETGs (see Sect. 6.4.2), and that  $s = -0.9$  as in Sect 6.1. To estimate  $f_{\text{sf}}$  we used the parametrisation of the gas fraction as a function of stellar mass and cosmic time provided by Rodrigues et al. (2012),

$$f_{\text{gas}}(z, M_{\star}) = \frac{M_{\text{gas}}}{M_{\star} + M_{\text{gas}}} = \frac{1}{1 + [M_{\star}/10^{A(t)}]^{B(t)}}, \quad (20)$$

where  $t$  is the cosmic time between redshift  $z$  and the present,

$$A(t) = 9.15 + 0.13t, \quad (21)$$

$$B(t) = 0.5 + 13.36 \times \exp(-38.02/t). \quad (22)$$

$A(t)$  represents the stellar mass at a given time for which the gas fraction is equal to 50%. The parameter increases linearly with lookback time.  $B(t)$  corresponds to the slope of the function. Then, we assumed the prescriptions in Hopkins et al. (2009) to estimate the amount of the initial gas mass that is transformed into stars during the merger,  $f_{\text{burst}} = f_{\text{gas}}(1 - f_{\text{gas}})2\mu/(1 + \mu)$ . Finally,

$$f_{\text{sf}} = M_{\text{burst}}/M_{\star} = \frac{2}{3}f_{\text{gas}}, \quad (23)$$

where the factor  $2/3$  is the efficiency for  $\mu = 1/2$  mergers, which is the typical major merger mass ratio (López-Sanjuan et al. 2011, 2012).

- The fraction of late-type galaxies (spirals and irregulars),  $f_{\text{LTG}}(z, M_{\star})$ , is the number of potential gas-rich merger progenitors over the total population. We parametrise this fraction as

$$f_{\text{LTG}}(z, M_{\star}) = 0.56 + 0.16z - 0.58[\log(M_{\star}/M_{\odot}) - 11]. \quad (24)$$



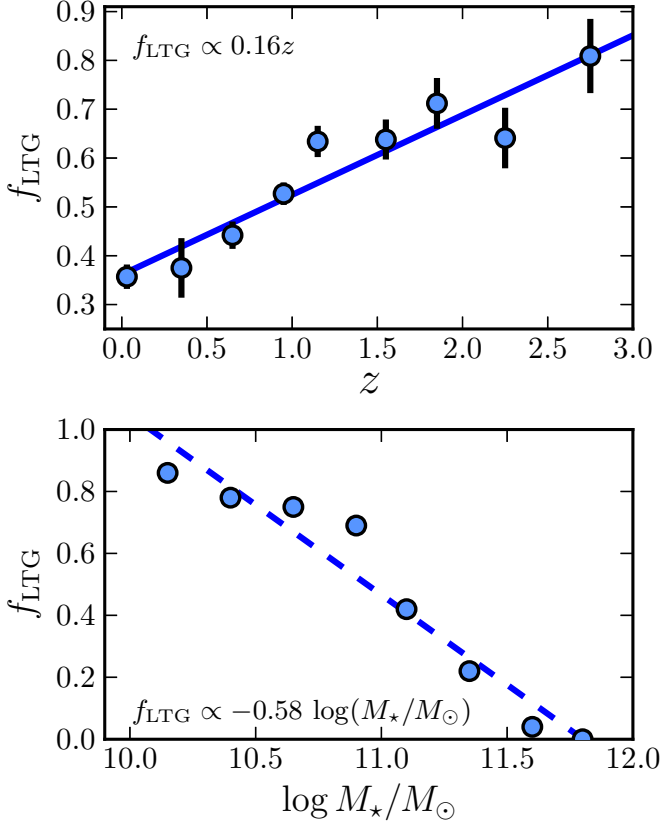


**Fig. 28.** Fraction of late-type galaxies as a function of redshift (top panel) and stellar mass at  $z \sim 0$  (bottom panel). The redshift data points are from Buitrago et al. (2013), and the stellar mass ones from Bernardi et al. (2010) in the SDSS. The line in both panels is the best least-squares linear fit to the data. [A colour version of this plot is available at the electronic edition].

We estimated the redshift dependence from the  $f_{\text{LTG}}$  reported by Buitrago et al. (2013) at  $z < 3$  (Fig. 28, top panel), and the mass dependence from the late-type fractions in the SDSS presented in Bernardi et al. (2010, Fig. 28, bottom panel). We assumed  $f_{\text{LTG}} = 1$  when Eq. (24) is higher than one, and  $f_{\text{LTG}} = 0$  when it is negative.

Finally, we define the fraction of new massive ETGs due to gas-rich (wet) mergers as

$$f_{\text{wet}}(z_{\text{min}}, z_{\text{max}}) = \frac{\rho_{\text{wet}}(z_{\text{min}}, z_{\text{max}}, 10^{11.25} M_{\odot})}{\rho_{\text{ETG}}(z_{\text{min}}) - \rho_{\text{ETG}}(z_{\text{max}})}. \quad (25)$$

Our merger model finds  $f_{\text{wet}}(0, 1.3) \sim 50\%$ , while this fraction increases up to  $f_{\text{wet}}(z, 1.3) \gtrsim 90\%$  when we focus on the high- $z$  regime,  $z \gtrsim 0.8$  (dashed line in Fig. 26). This indicates that gas-rich major mergers are common enough at  $z \gtrsim 0.8$  to explain the observed increase in the number density of massive ETGs. However, at  $z \lesssim 0.8$  only one third of the evolution can be accounted by these mergers,  $f_{\text{wet}}(0, 0.8) \sim 40\%$ . That supports the idea that gas-rich major merging is the main process involved in the assembly of the red sequence at  $z \gtrsim 1$  (e.g., Ilbert et al. 2010; López-Sanjuan et al. 2010b; Eliche-Moral et al. 2010; Prieto et al. 2013).

In addition to wet mergers, dry mergers can also increase the number density of massive ETGs. In this case they promote ETGs with  $M_{\star} < 10^{11.25} M_{\odot}$  to the massive regime. We estimate the contribution of both major and minor dry mergers as

$$\rho_{\text{dry}}^{+}(z_{\text{min}}, z_{\text{max}}, M_{\star, \text{lim}}) = \int_{z_1}^{z_2} \int_0^{M_{\star, \text{lim}}} \Phi R_{\text{MM}}^{\text{ETG}} E_{\text{MM}} f_{\text{ETG}} dM_{\star} dz + \int_{z_1}^{z_2} \int_0^{M_{\star, \text{lim}}} \Phi R_{\text{mm}}^{\text{ETG}} E_{\text{mm}} f_{\text{ETG}} dM_{\star} dz, \quad (26)$$

where  $R_{\text{MM}}^{\text{ETG}}$  ( $R_{\text{mm}}^{\text{ETG}}$ ) is the major (minor) merger rate of massive ETGs galaxies from López-Sanjuan et al. (2012),  $f_{\text{ETG}} = 1 - f_{\text{LTG}}$ , the minor merger efficiency function is defined as  $E_{\text{mm}} \equiv E(z, M_{\star}, M_{\star, \text{lim}}, \mu_{\text{max}} = 1/4, \mu_{\text{min}} = 1/10)$ , and we assumed  $f_{\text{sf}} = 0$  in both major and minor merger efficiency functions. Note that the integration in mass space only reach  $M_{\star, \text{lim}}$  and that the merger rates from López-Sanjuan et al. (2012) include also mixed mergers (ETGs - LTGs). However, dry mergers between two already massive ETGs decrease the number density  $\rho_{\text{ETG}}$ . We take this into account with the following function,

$$\rho_{\text{dry}}^{-}(z_{\text{min}}, z_{\text{max}}, M_{\star, \text{lim}}) = \int_{z_1}^{z_2} \int_{M_{\star, \text{lim}}}^{\infty} \Phi R_{\text{MM}}^{\text{ETG}} \epsilon_{\text{MM}} f_{\text{ETG}} dM_{\star} dz + \int_{z_1}^{z_2} \int_{M_{\star, \text{lim}}}^{\infty} \Phi R_{\text{mm}}^{\text{ETG}} \epsilon_{\text{mm}} f_{\text{ETG}} dM_{\star} dz, \quad (27)$$

where in this case the merger efficiency function has the form

$$\epsilon = \begin{cases} 0.65, & \text{if } M_{\star} \geq M_{\star, 3}, \\ 0.65 \times (\mu/\mu_{\text{min}})^s & \text{if } M_{\star, 4} \leq M_{\star} < M_{\star, 3}, \\ 0, & \text{if } M_{\star} < M_{\star, 4}, \end{cases} \quad (28)$$

where

$$M_{\star, 3} = \mu_{\text{min}}^{-1} M_{\star, \text{lim}}, \quad (29)$$

$$M_{\star, 4} = \mu_{\text{max}}^{-1} M_{\star, \text{lim}}, \quad (30)$$

$$\mu = \frac{M_{\star, \text{lim}}}{M_{\star}}. \quad (31)$$

and the factor 0.65 is the fraction of companions of massive galaxies that are already early-type/red galaxies (López-Sanjuan et al. 2012; Newman et al. 2012a). As previously, we define the major merger efficiency as  $\epsilon_{\text{MM}} \equiv \epsilon(z, M_{\star}, M_{\star, \text{lim}}, \mu_{\text{max}} = 1, \mu_{\text{min}} = 1/4)$  and the minor merger efficiency as  $\epsilon_{\text{mm}} \equiv \epsilon(z, M_{\star}, M_{\star, \text{lim}}, \mu_{\text{max}} = 1/4, \mu_{\text{min}} = 1/10)$ .

Analogous to the wet merger case, we define

$$f_{\text{dry}}(z_{\text{min}}, z_{\text{max}}) = \frac{\rho_{\text{dry}}(z_{\text{min}}, z_{\text{max}}, 10^{11.25} M_{\odot})}{\rho_{\text{ETG}}(z_{\text{min}}) - \rho_{\text{ETG}}(z_{\text{max}})} = \frac{\rho_{\text{dry}}^{+}(z_{\text{min}}, z_{\text{max}}, 10^{11.25} M_{\odot}) - \rho_{\text{dry}}^{-}(z_{\text{min}}, z_{\text{max}}, 10^{11.25} M_{\odot})}{\rho_{\text{ETG}}(z_{\text{min}}) - \rho_{\text{ETG}}(z_{\text{max}})} \quad (32)$$

to explore the role of dry mergers in massive ETGs assembly since  $z = 1.3$ . We find  $f_{\text{dry}}(0, 1.3) \sim 40\%$ . As shown in Fig. 26, dry mergers are more important at recent cosmic times due to the increase in the number density of ETGs, in contrast with the diminishing importance of gas-rich mergers. For example, we have  $f_{\text{dry}}(0.8, 1.3) \sim 15\%$ , while  $f_{\text{dry}}(0, 0.8) \sim 45\%$ .

The combined effect of gas-rich and dry mergers,  $f_{\text{tot}} = f_{\text{wet}} + f_{\text{dry}}$ , is able to explain most of the evolution in  $\rho_{\text{ETG}}$  since  $z = 1.3$ , with  $f_{\text{tot}}(0, 1.3) \sim 90\%$ . Thus, our model suggests merging as the main process in the assembly of massive ETGs since  $z = 1.3$ . Two thirds of the number density evolution is due to gas-rich major mergers, while one third is coming from major and minor dry mergers.

The measurement of the merger rate at  $z \gtrsim 1.5$  is needed to fully constraint the role of gas-rich major mergers in the early assembly of the red sequence, as well as the possible contribution of cold gas accretion in this mass assembly.

#### 6.4.1. Fast and slow rotators in the local universe

The results from the SAURON project (de Zeeuw et al. 2002) propose a kinematical classification of morphological ETGs into fast and slow rotators (Emsellem et al. 2007). Recently, the ATLAS<sup>3D,9</sup> (Cappellari et al. 2011) survey has observed a representative sample of 260 nearby ETGs, finding that the fraction of slow rotators increases with the dynamical mass (Emsellem et al. 2011). The cosmological simulation analysed by Khochfar et al. (2011) suggests that the main difference between fast and slow rotators is their average number of major mergers, with fast rotators having undergone one major merger, while slow rotators have undergone two. We use this fact and the merging model developed in the previous section, to predict the fraction of slow rotators in the local universe,  $f_{\text{slow}}$ . We simply assumed that wet major mergers produce fast rotators (first major merger event), dry major mergers produce slow rotators (second major merger event), and dry minor mergers do not change the kinematical state of ETGs. In addition, we took all the ETGs at  $z = 1.3$  as fast rotators.

With the previous assumptions, we expect  $f_{\text{slow}} \sim 60\%$ , in good agreement with the ATLAS<sup>3D</sup> result of  $f_{\text{slow}} \sim 47 - 75\%$  for ETGs with a dynamical mass  $M_{\text{dyn}} \geq 10^{11.25} M_{\odot}$  (Emsellem et al. 2011). Thus, our model also reproduces the local fraction of slow/fast rotators of massive ETGs galaxies, reinforcing the conclusions of the previous section.

#### 6.4.2. Uncertainties in the model

The model presented in previous sections has set most of its parameters from observational results. However, there are two unconstrained parameters that could affect our conclusions. The first parameter is  $f_{\text{disc}}$ , the fraction of gas-rich major mergers whose remnant rebuild a disc component and do not contribute to the increase in  $\rho_{\text{ETG}}$ . We assumed  $f_{\text{disc}} = 0$ , and in the following we justify this selection. Hopkins et al. (2009) find that a high gas fraction prevents the destruction of the disc component after a major merger in their  $N$ -body/hydrodynamical simulations (but see Bournaud et al. 2011 for a different point of view). These simulations suggest that disc rebuild could be an efficient process when the gas fraction is  $f_{\text{gas}} \gtrsim 50\%$ . However, we have focused in the massive end of the galaxy population, where the gas fractions are lower. Thanks to Eq. (20), we can estimate the gas fraction of the gas-rich mergers in our model. We find  $f_{\text{gas}} \lesssim 30\%$ , justifying the assumed  $f_{\text{disc}} = 0$ . At lower masses than explored in the present section, the gas fraction is higher, and disc rebuild could be an important process in the formation of bulge-dominated spirals (e.g., Huertas-Company et al. 2010; Puech et al. 2012). However, we cannot discard positive values of  $f_{\text{disc}}$  for massive galaxies, as we see below.

The second parameter is the assumed merger time scale, which typically has a factor of two uncertainty in their normalization (e.g., Hopkins et al. 2010). The  $T_{\text{MM}}$  from Kitzbichler & White (2008) are typically longer than others in the literature (e.g., Patton & Atfield 2008; Lin et al. 2010) or similar to those from  $N$ -body/hydrodynamical simulations (Lotz et al. 2010b,a). Thus, we expect, if anything, a shorter  $T_{\text{MM}}$ , which implies a larger number density of ETGs due to mergers. Nevertheless, the good description of the  $\rho_{\text{ETG}}$  evolution with our merger model strongly suggests that mergers are indeed the main process in massive ETGs assembly. Thus, a lower  $T_{\text{MM}}$  (i.e., a higher merger rate that translates to an ex-

cess of ETGs) could be compensated by a positive value of  $f_{\text{disc}}$ , that reduces the number density of ETGs due to mergers.

Future observational studies will be important to better constraint the parameters of our model, and further theoretical efforts are needed to understand the uncertainties in the assumed parameters.

## 7. Summary and conclusions

Using SINFONI/VLT 3D spectroscopy, we have been able to measure, for the first time with spectroscopically-confirmed close pairs, the gas-rich major merger fraction and merger rate at around the peak in star formation activity at  $0.9 < z < 1.8$ , from the MASSIV sample of star-forming galaxies with a stellar mass range  $M_{\star} = 10^9 - 10^{11} M_{\odot}$ . In this redshift range we identify 20 close pairs, and classify 13 as major mergers based on a separation  $r_p \leq 20h^{-1} - 30h^{-1}$  kpc and a relative velocity  $\Delta v \leq 500 \text{ km s}^{-1}$ .

We find that the gas-rich major merger fraction is high,  $20.8^{+15.2}_{-6.8}\%$ ,  $20.1^{+8.0}_{-5.1}\%$ , and  $22.0^{+13.7}_{-7.3}\%$  for  $r_p \leq 20h^{-1}$  kpc close pairs in redshift ranges  $z = [0.94, 1.06]$ ,  $[1.2, 1.5]$ , and  $[1.5, 1.8]$ , respectively. When compared to measurements at redshifts  $z < 1$ , the evolution of the (gas-rich) merger fraction can be parametrised as  $f_{\text{MM}} = 0.0066 \times (1+z)^m$  with  $m = 3.91 \pm 0.16$ . We note that the evolution between  $z = 1$  and  $z \sim 1.5$  seems to flatten out compared to lower redshifts.

The merger rate has been derived using merger time scales from the literature: we find that the gas-rich merger rate is  $0.116^{+0.084}_{-0.038} \text{ Gyr}^{-1}$ ,  $0.147^{+0.058}_{-0.037} \text{ Gyr}^{-1}$ , and  $0.127^{+0.079}_{-0.042} \text{ Gyr}^{-1}$  at  $z = 1.03, 1.32$ , and  $1.54$ , respectively, for merger time scales of  $T_{\text{MM}} \sim 1.5 \text{ Gyr}$ . We then find that the (gas-rich) merger rate's evolution for galaxies with stellar mass  $\overline{M}_{\star} = 10^{10-10.5} M_{\odot}$  over  $z = [0, 1.5]$  scales as  $(1+z)^n$  with  $n = 3.95 \pm 0.12$ .

Using these measurements, we developed a simple model to estimate the contribution of gas-rich major mergers to the growth of galaxies on the red sequence. We infer that  $\sim 35\%$  of the star-forming galaxies with stellar mass  $\overline{M}_{\star} = 10^{10} - 10^{10.5} M_{\odot}$  have undergone a major merger since  $z \sim 1.5$ . The number of major merger events was about 5 times higher at  $1 < z < 1.5$  compared to  $z < 1$ . Assuming that each gas-rich major merger produces a new early-type galaxy, we infer that the number of gas-rich major mergers is large enough at  $z > 1$  to explain the increase in the number density of massive ETGs, supporting a picture where gas-rich (wet) merging is the main process building-up the red sequence. While gas-rich mergers become rarer towards lower redshifts, the number of dry mergers is steadily increasing, and the combination of these two processes accounts for most, if not all, of the increase in the number density of massive ETGs since  $z \sim 1.3$ . Two-thirds of this number density evolution is due to wet major mergers, while one-third is coming from major and minor dry mergers. These results add further evidence to a picture where merging is a major process driving mass assembly into the massive red sequence galaxies.

We note that minor merging is definitely present in the MASSIV sample (see Sect. 4). However, due to incompleteness in detecting these faint companions, we are not able to assess a minor merger rate at these epochs from our data. In the global picture of red sequence assembly, we emphasise that a simple extrapolation of the minor merger rate measured up to  $z \sim 1$  by López-Sanjuan et al. (2011), would indicate that from  $z \sim 1.5$  to the present, minor mergers with  $1/10 \leq \mu < 1/4$  are not common enough to significantly move spiral galaxies into the red sequence.

<sup>9</sup> <http://www-astro.physics.ox.ac.uk/atlas3d/>

To get a complete picture of the life-time effect of major merging on massive galaxies, accurate measurements of the merger fraction and merger rate are needed beyond  $z \sim 2$ . Spectroscopic surveys will remain an important element to provide secure identification of merging systems at these early epochs.

*Acknowledgements.* We dedicate this paper to the memory of our six IAC colleagues and friends who met with a fatal accident in Piedra de los Cochinos, Tenerife, in February 2007, with a special thanks to Maurizio Panniello, whose teachings of python were so important for this paper.

We thank the comments and suggestions of the anonymous referee, and L. Pozzetti and F. Buitrago for kindly provide their number densities. This work has been supported by funding from ANR-07-BLAN-0228 and ERC-2010-AdG-268107-EARLY and partially supported by the CNRS-INSU and its Programme National Cosmologie-Galaxies (France) and by the French ANR grant ANR-07-JCJC-0009.

## References

- Abazajian, K. N., Adelman-McCarthy, J. K., Agüeros, M. A., et al. 2009, *ApJS*, 182, 543
- Arnouts, S., Walcher, C. J., Le Fèvre, O., et al. 2007, *A&A*, 476, 137
- Bell, E. F., Phleps, S., Somerville, R. S., et al. 2006, *ApJ*, 652, 270
- Bernardi, M., Shankar, F., Hyde, J. B., et al. 2010, *MNRAS*, 404, 2087
- Bielby, R., Hudelot, P., McCracken, H. J., et al. 2012, *A&A*, 545, A23
- Bluck, A. F. L., Conselice, C. J., Bouwens, R. J., et al. 2009, *MNRAS*, 394, L51
- Bluck, A. F. L., Conselice, C. J., Buitrago, F., et al. 2012, *ApJ*, 747, 34
- Bournaud, F., Chapon, D., Teyssier, R., et al. 2011, *ApJ*, 730, 4
- Bridge, C. R., Carlberg, R. G., & Sullivan, M. 2010, *ApJ*, 709, 1067
- Bruzual, G. & Charlot, S. 2003, *MNRAS*, 344, 1000
- Buitrago, F., Trujillo, I., Conselice, C. J., & Häußler, B. 2013, *MNRAS*, 428, 1460
- Bundy, K., Fukugita, M., Ellis, R. S., et al. 2009, *ApJ*, 697, 1369
- Cameron, E. 2011, *PASA*, 28, 128
- Cameron, E. & Pettitt, A. N. 2012, *MNRAS*, 425, 44
- Cappellari, M., Emsellem, E., Krajnović, D., et al. 2011, *MNRAS*, 413, 813
- Chou, R. C. Y., Bridge, C. R., & Abraham, R. G. 2011, *AJ*, 141, 87
- Conselice, C. J. 2003, *ApJS*, 147, 1
- Conselice, C. J. 2006, *ApJ*, 638, 686
- Conselice, C. J., Bluck, A. F. L., Buitrago, F., et al. 2011a, *MNRAS*, 413, 80
- Conselice, C. J., Bluck, A. F. L., Ravindranath, S., et al. 2011b, *MNRAS*, 417, 2770
- Conselice, C. J., Bundy, K., Trujillo, I., et al. 2007, *MNRAS*, 381, 962
- Conselice, C. J., Rajgor, S., & Myers, R. 2008, *MNRAS*, 386, 909
- Contini, T., Garilli, B., Le Fèvre, O., et al. 2012, *A&A*, 539, A91
- Cucciati, O., Marinoni, C., Iovino, A., et al. 2010, *A&A*, 520, A42
- Cucciati, O., Tresse, L., Ilbert, O., et al. 2012, *A&A*, 539, A31
- Darg, D. W., Kaviraj, S., Lintott, C. J., et al. 2010, *MNRAS*, 401, 1043
- De Propriis, R., Conselice, C. J., Liske, J., et al. 2007, *ApJ*, 666, 212
- de Ravel, L., Kampczyk, P., Le Fèvre, O., et al. 2011, *A&A*, submitted [ArXiv: 1104.5470]
- de Ravel, L., Le Fèvre, O., Tresse, L., et al. 2009, *A&A*, 498, 379
- de Zeeuw, P. T., Bureau, M., Emsellem, E., et al. 2002, *MNRAS*, 329, 513
- Dekel, A. & Birnboim, Y. 2006, *MNRAS*, 368, 2
- Domingue, D. L., Xu, C. K., Jarrett, T. H., & Cheng, Y. 2009, *ApJ*, 695, 1559
- Dye, S., Warren, S. J., Hambly, N. C., et al. 2006, *MNRAS*, 372, 1227
- Eliche-Moral, M. C., Prieto, M., Gallego, J., et al. 2010, *A&A*, 519, A55
- Emsellem, E., Cappellari, M., Krajnović, D., et al. 2011, *MNRAS*, 414, 888
- Emsellem, E., Cappellari, M., Krajnović, D., et al. 2007, *MNRAS*, 379, 401
- Epinat, B., Tasca, L., Amram, P., et al. 2012, *A&A*, 539, A92
- Förster Schreiber, N. M., Genzel, R., Bouché, N., et al. 2009, *ApJ*, 706, 1364
- Franzetti, P., Scodreggio, M., Garilli, B., Fumana, M., & Paiono, L. 2008, in *Astronomical Society of the Pacific Conference Series*, Vol. 394, *Astronomical Data Analysis Software and Systems XVII*, ed. R. W. Argyle, P. S. Bunclark, & J. R. Lewis, 642
- Garilli, B., Le Fèvre, O., Guzzo, L., et al. 2008, *A&A*, 486, 683
- Giavalisco, M., Ferguson, H. C., Koekemoer, A. M., et al. 2004, *ApJ*, 600, L93
- Goranova, Y., Hudelot, P., Magnard, F., et al. 2009, the CFHTLS T0006 Release
- Hopkins, P. F., Cox, T. J., Younger, J. D., & Hernquist, L. 2009, *ApJ*, 691, 1168
- Hopkins, P. F., Croton, D., Bundy, K., et al. 2010, *ApJ*, 724, 915
- Hopkins, P. F., Hernquist, L., Cox, T. J., Dutta, S. N., & Rothberg, B. 2008, *ApJ*, 679, 156
- Huertas-Company, M., Aguerri, J. A. L., Tresse, L., et al. 2010, *A&A*, 515, A3
- Ilbert, O., Lauger, S., Tresse, L., et al. 2006, *A&A*, 453, 809
- Ilbert, O., Salvato, M., Le Flocc'h, E., et al. 2010, *ApJ*, 709, 644
- Jogee, S., Miller, S. H., Penner, K., et al. 2009, *ApJ*, 697, 1971
- Khochfar, S., Emsellem, E., Serra, P., et al. 2011, *MNRAS*, 417, 845
- Kitzbichler, M. G. & White, S. D. M. 2008, *MNRAS*, 380
- Law, D. R., Steidel, C. C., Erb, D. K., et al. 2009, *ApJ*, 697, 2057
- Law, D. R., Steidel, C. C., Erb, D. K., et al. 2007, *ApJ*, 656, 1
- Law, D. R., Steidel, C. C., Shapley, A. E., et al. 2012, *ApJ*, 745, 85
- Le Fèvre, O., Abraham, R., Lilly, S. J., et al. 2000, *MNRAS*, 311, 565
- Le Fèvre, O., Vettolani, G., Garilli, B., et al. 2005, *A&A*, 439, 845
- Le Fèvre, O., Vettolani, G., Paltani, S., et al. 2004, *A&A*, 428, 1043
- Lilly, S. J., Le Fèvre, O., Renzini, A., et al. 2007, *ApJS*, 172, 70
- Lin, L., Cooper, M. C., Jian, H., et al. 2010, *ApJ*, 718, 1158
- Lin, L., Koo, D. C., Willmer, C. N. A., et al. 2004, *ApJ*, 617, L9
- Lin, L., Patton, D. R., Koo, D. C., et al. 2008, *ApJ*, 681, 232
- López-Sanjuan, C., Balcells, M., García-Dabó, C. E., et al. 2009a, *ApJ*, 694, 643
- López-Sanjuan, C., Balcells, M., Pérez-González, P. G., et al. 2010a, *A&A*, 518, A20
- López-Sanjuan, C., Balcells, M., Pérez-González, P. G., et al. 2009b, *A&A*, 501, 505
- López-Sanjuan, C., Balcells, M., Pérez-González, P. G., et al. 2010b, *ApJ*, 710, 1170
- López-Sanjuan, C., García-Dabó, C. E., & Balcells, M. 2008, *PASP*, 120, 571
- López-Sanjuan, C., Le Fèvre, O., de Ravel, L., et al. 2011, *A&A*, 530, A20
- López-Sanjuan, C., Le Fèvre, O., Ilbert, O., et al. 2012, *A&A*, 548, A7
- Lotz, J. M., Jonsson, P., Cox, T. J., et al. 2011, *ApJ*, 742, 103
- Lotz, J. M., Jonsson, P., Cox, T. J., & Primack, J. R. 2008, *MNRAS*, 391, 1137
- Lotz, J. M., Jonsson, P., Cox, T. J., & Primack, J. R. 2010a, *MNRAS*, 404, 590
- Lotz, J. M., Jonsson, P., Cox, T. J., & Primack, J. R. 2010b, *MNRAS*, 404, 575
- Maiolino, R., Nagao, T., Grazian, A., et al. 2008, *A&A*, 488, 463
- Man, A. W. S., Toft, S., Zirm, A. W., Wuyts, S., & van der Wel, A. 2012, *ApJ*, 744, 85
- Mannucci, F., Cresci, G., Maiolino, R., et al. 2009, *MNRAS*, 398, 1915
- Mármol-Queraltó, E., Trujillo, I., Pérez-González, P. G., Varela, J., & Barro, G. 2012, *MNRAS*, 422, 2187
- Naab, T., Jesseit, R., & Burkert, A. 2006, *MNRAS*, 372, 839
- Newman, A. B., Ellis, R. S., Bundy, K., & Treu, T. 2012a, *ApJ*, 746, 162
- Newman, J. A., Cooper, M. C., Davis, M., et al. 2012b, *ArXiv e-prints*
- Patton, D. R. & Atfield, J. E. 2008, *ApJ*, 685, 235
- Patton, D. R., Carlberg, R. G., Marzke, R. O., et al. 2000, *ApJ*, 536, 153
- Patton, D. R., Pritchett, C. J., Yee, H. K. C., Ellingson, E., & Carlberg, R. G. 1997, *ApJ*, 475, 29
- Peng, C. Y., Ho, L. C., Impey, C. D., & Rix, H.-W. 2002, *AJ*, 124, 266
- Peng, C. Y., Ho, L. C., Impey, C. D., & Rix, H.-W. 2010, *AJ*, 139, 2097
- Pérez-González, P. G., Rieke, G. H., Villar, V., et al. 2008, *ApJ*, 675, 234
- Pozzetti, L., Bolzonella, M., Zucca, E., et al. 2010, *A&A*, 523, A13
- Prieto, M., Eliche-Moral, M. C., Balcells, M., et al. 2013, *MNRAS*, 428, 999
- Puech, M., Hammer, F., Hopkins, P. F., et al. 2012, *ApJ*, 753, 128
- Queyrel, J., Contini, T., Kissler-Patig, M., et al. 2012, *A&A*, 539, A93
- Robaina, A. R., Bell, E. F., van der Wel, A., et al. 2010, *ApJ*, 719, 844
- Rodrigues, M., Puech, M., Hammer, F., Rothberg, B., & Flores, H. 2012, *MNRAS*, 421, 2888
- Rothberg, B. & Fischer, J. 2010, *ApJ*, 712, 318
- Rothberg, B. & Joseph, R. D. 2006a, *AJ*, 131, 185
- Rothberg, B. & Joseph, R. D. 2006b, *AJ*, 132, 976
- Ryan, Jr., R. E., Cohen, S. H., Windhorst, R. A., & Silk, J. 2008, *ApJ*, 678, 751
- Salpeter, E. E. 1955, *ApJ*, 121, 161
- Scoville, N., Aussel, H., Brusa, M., et al. 2007, *ApJS*, 172, 1
- Sérsic, J. L. 1968, *Atlas de galaxies australes (Cordoba, Argentina: Observatorio Astronomico)*, 1968)
- Springel, V., White, S. D. M., Jenkins, A., et al. 2005, *Nature*, 435, 629
- van der Wel, A., Rix, H.-W., Wuyts, S., et al. 2011, *ApJ*, 730, 38
- van Dokkum, P. G., Brammer, G., Fumagalli, M., et al. 2011, *ApJ*, 743, L15
- Vergani, D., Epinat, B., Contini, T., et al. 2012, *A&A*, 546, A118
- Vergani, D., Scodreggio, M., Pozzetti, L., et al. 2008, *A&A*, 487, 89
- Walcher, C. J., Lamareille, F., Vergani, D., et al. 2008, *A&A*, 491, 713
- Williams, R. J., Quadri, R. F., & Franx, M. 2011, *ApJ*, 738, L25
- Xu, C. K., Zhao, Y., Scoville, N., et al. 2012, *ApJ*, 747, 85
- Yang, Y., Flores, H., Hammer, F., et al. 2008, *A&A*, 477, 789
- Zucca, E., Ilbert, O., Bardelli, S., et al. 2006, *A&A*, 455, 879

## Appendix A: Spectroscopic Success Rate in the VVDS-Wide fields

We computed the Spectroscopic Success Rate (*SSR*) in the VVDS-Wide 14h and 22h fields for a given redshift range by following the prescriptions in Ilbert et al. (2006): we compared

the number of galaxies with flag = 4, 3 and 2 over the total number of galaxies (those with flag = 4, 3, 2, 1 and 0). Because flag = 1 galaxies have a 50% reliability and no redshift information is available for flag = 0 galaxies, we took advantage of the latest photometric redshifts from CFHTLS survey to estimate the number of galaxies with flag = 1 and 0 that belong to the redshift range of interest. With the previous steps we estimate the  $SSR$  in the 22h field as

$$SSR_{22h}(z_r) = \frac{N_{22h,spec}(z_r)}{N_{22h,spec}(z_r) + N_{22h,phot}(z_r)}, \quad (\text{A.1})$$

where  $N_{22h,spec}(z_r)$  is the number of galaxies with flag = 4, 3 and 2 in the redshift range  $z_r$ , and  $N_{22h,phot}(z_r)$  is the number of galaxies with flag = 1 and 0, and with a photometric redshift in the same redshift range. As the available imaging data in the 14h field is not as deep as the CFHTLS, we show in the following that we can assume that the  $SSR$  in the 14h field follows the same distribution as in the 22h field, for which CFHTLS photometry is available.

First we checked the properties of the stars in these two VVDS-Wide fields. The fraction of stars in the 22h (14h) field is 66% (51%) for flag = 4 sources, 38% (26%) for flag = 3 sources, 24% (23%) for flag = 2 sources, and 11% (12%) for flag = 1 sources. So the fraction of stars is similar in both fields for flag = 2 and 1 sources, while higher in the 22h field for flag = 4 and 3. We checked that the normalised distributions of the VVDS-Wide stars as a function of their observed  $I_{AB}$ -band magnitude in both fields are similar for each flag. We note that stars with high confidence flag are brighter than the low confidence ones, as expected. The fraction of bright stars ( $I_{AB} \leq 21$ ) in the 22h (14h) field is 75% (67%) for flag = 4 stars, 49% (43%) for flag = 3 stars, 30% (29%) for flag = 2 stars, and 19% (16%) for flag = 1 stars. These fractions suggest that there is a higher density of bright stars in the 22h area than in the 14h one, that translates in a higher fraction of stars for flag = 4 and 3 sources, while faint stars have similar densities in both fields, leading to a similar fraction of stars with flag = 2 and 1. Because of this, we assumed that the fraction of stars among flag = 0 sources, that we estimate in the 22h field from the CFHTLS photometry, is similar in 22h and 14h fields.

The distribution of galaxies at  $z \geq 0.9$ , the redshift range in which we are interested on, are also similar in both fields. Because of this, we assumed that the photometric distribution of galaxies with flag = 1 and 0 is similar in both fields, and we use those in 22h field to estimate  $N_{14h,phot}$  and the  $SSR$  in the 14h field:

$$SSR_{14h}(z_r) = \frac{N_{14h,spec}(z_r)}{N_{14h,spec}(z_r) + f_{22h}(z_r) \times n_{14h}(1, 0)}, \quad (\text{A.2})$$

where  $n_{14h}(1, 0)$  is the total number of sources (galaxies and stars) with flag = 1 and 0 in the 14h field, and  $f_{22h}(z_r) = N_{22h,phot}(z_r)/n_{22h}(1, 0)$  is the fraction of sources with a photometric redshift in the redshift range  $z_r$  over the total population of sources with flag = 1 and 0 in the 22h field.

## Appendix B: GALFIT residual images of blended MASSIV close pairs

In this Appendix we detail the modelling in the  $i$  band of those MASSIV close pair candidates with overlapping components in the kinematical maps. We used GALFIT v3.0 (Peng et al. 2010) to model the light distribution with two independent Sérsic components. We set the initial positions of the sources using the information from the kinematical maps, and we did not impose any

constraint on the other initial parameters of the fit (i.e., luminosity, effective radius, Sérsic index, position angle and inclination). Because of the minimisation process performed by GALFIT in the fitting, the best model with two components should not be unique and the convergence to a given solution should depend on the initial values of the parameters defined by the user. We checked, by exploring randomly the space of initial values, that the number of good solutions is at most two. Where two good solutions exist, the one that better reproduces both the velocity field and the velocity dispersion map is preferred. To illustrate the need of a second component to describe the blended close pair systems in MASSIV, we show in Fig. B.1 the original image in the  $i$  band and the residual image from GALFIT with one and two components. In all the cases the residual map from the one component fit suggests that a second component is present. This Figure also demonstrates that both the seeing ( $\sim 0.7''$ ) and the depth of the  $i$ -band images used in the present study are good enough to characterise sources with two overlapping components.

## Appendix C: Completeness of the close pair sample

Throughout the present paper we have assumed that the close pair systems detected in the MASSIV sample are representative for galaxies with  $I_{AB} \leq 23.9$ . The MASSIV sample comprises galaxies fainter than this luminosity limit, and in this appendix we justify the boundary applied in our analysis.

The VVDS parent samples of the MASSIV sample are randomly selected in the  $I_{AB}$  band (Le Fèvre et al. 2005). Because of this, we studied the distribution of MASSIV sources as a function of the  $I_{AB}$ -band magnitude to obtain clues about the completeness of the MASSIV sample in our close pair study. We show the cumulative distribution of all MASSIV sources and of those with a close companion (both major and no major) in the top panel of Fig. C.1. Obviously, we are able to detect single MASSIV galaxies at fainter magnitudes than the close pairs ( $I_{AB} = 24.4$  vs 23.8) because in the latter case we have to detect both the principal source and the companion galaxy, which is usually fainter.

Lets assume for a moment that the detection curve of the MASSIV sources is a step function that is 1 for  $I_{AB} \leq I_{AB,lim}$  and 0 for fainter magnitudes. In this ideal case,  $I_{AB,lim}$  is defined by the fainter galaxy (close pair) detected. Thus, we should only be able to detect close pairs at  $I_{AB} \leq 23.8$ , and the measured merger fraction in the total MASSIV sample ( $I_{AB} \leq 24.4$ ) will be lower than the real merger fraction because of the missing faint close pairs with  $I_{AB} > 23.8$ . Of course, the detection curve in the MASSIV sample is more complicated than a step function, and could depend on redshift, geometry, luminosity, etc. Instead of trying to estimate the detection curve for MASSIV sources and for close companions to recover statistically the missing close pairs (see Patton et al. 2000; de Ravel et al. 2009, for examples of this kind of correction), we define the  $I_{AB}$ -band magnitude up to which the detected close pairs are representative of the total MASSIV sample, named  $I_{AB,comp}$ , and in our study we only keep those sources brighter than  $I_{AB,comp}$  to ensure reliable merger fractions.

The MASSIV sample is a representative subsample of the global star-forming population (Contini et al. 2012), and we expect the MASSIV galaxy pairs to be also a random sample of this global population. Therefore, the distributions in the  $I_{AB}$  band of the total and the close pair MASSIV sources should be similar when the close pairs detection was slightly affected by incompleteness issues. Following this idea, we performed



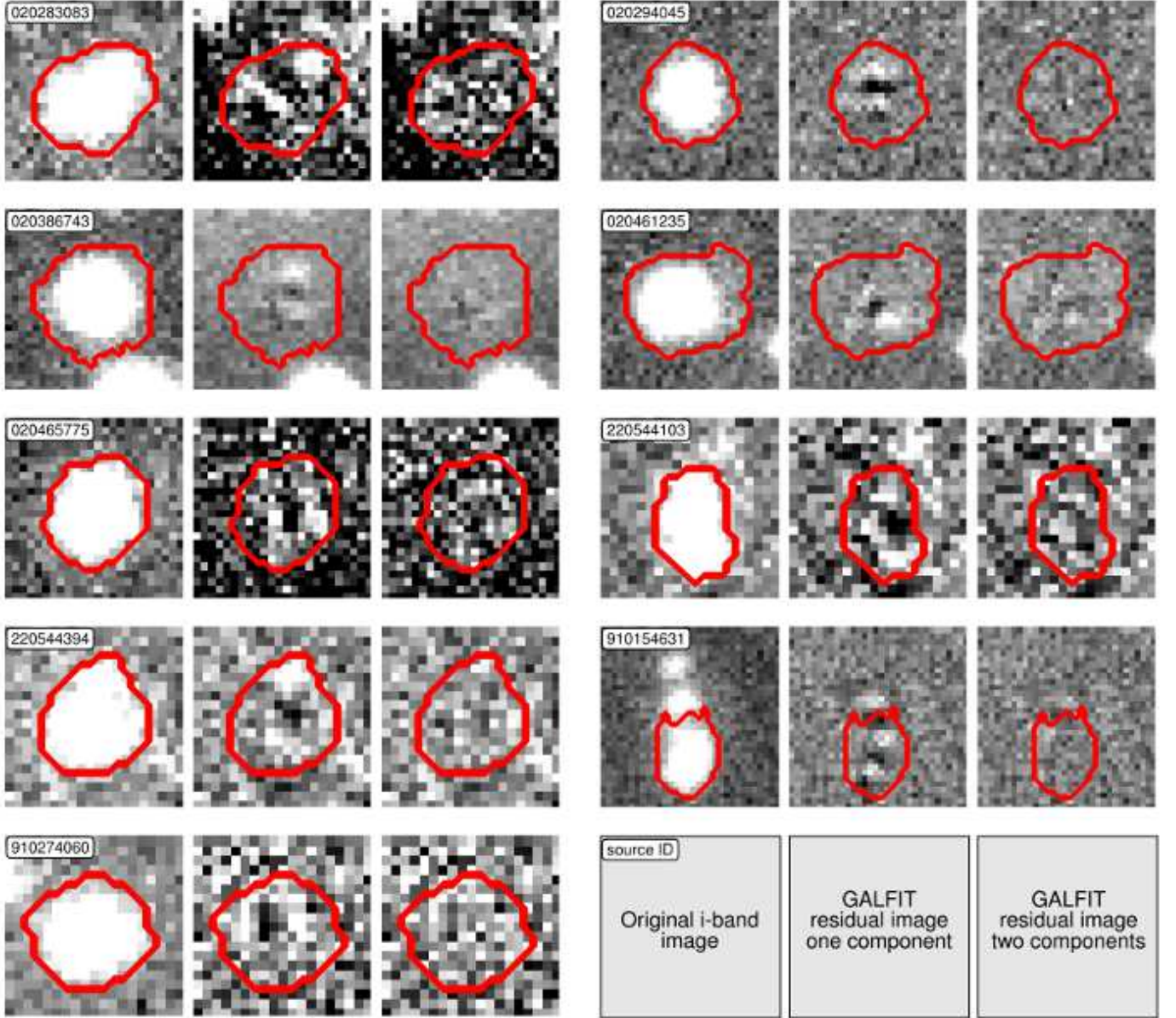


**Fig. B.1.** Original  $i$ -band image (left panels) and residual images from the GALFIT fit with one (central panels) and two components (right panels) of those MASSIV close pair candidates with overlapping components in the kinematical maps. The grey scale has been chosen to enhance the light residuals in the images. The solid contour marks the targeted MASSIV source to guide the eye. The ID of the showed MASSIV source is labelled in each left panel. [A colour version of this plot is available at the electronic edition].

a Kolmogorov-Smirnov (KS) test over the total and close pair MASSIV galaxies with  $I_{AB} \leq I_{AB,lim}$ , and explored different values of  $I_{AB,lim}$ , from 23.0 to 24.5. Then, the completeness magnitude  $I_{AB,comp}$  was defined by the minimum in the KS estimator  $D$ , i.e., where both distributions have the lower probability to be different. This exercise provides the curve in the bottom panel of Fig. C.1, that states  $I_{AB,comp} = 23.9$ . We repeated this procedure with the major merger sample, and we obtain a similar distribution of  $D$  values, reinforcing our choice.

In summary, in the estimation of the merger fraction we only use those MASSIV galaxies with  $I_{AB} \leq I_{AB,comp} = 23.9$ . This ensures that the close pair sample is a random subsample of the total MASSIV one, and we avoid any bias related with the shal-

lower detection curve of close pairs compared with that of the total MASSIV sample.



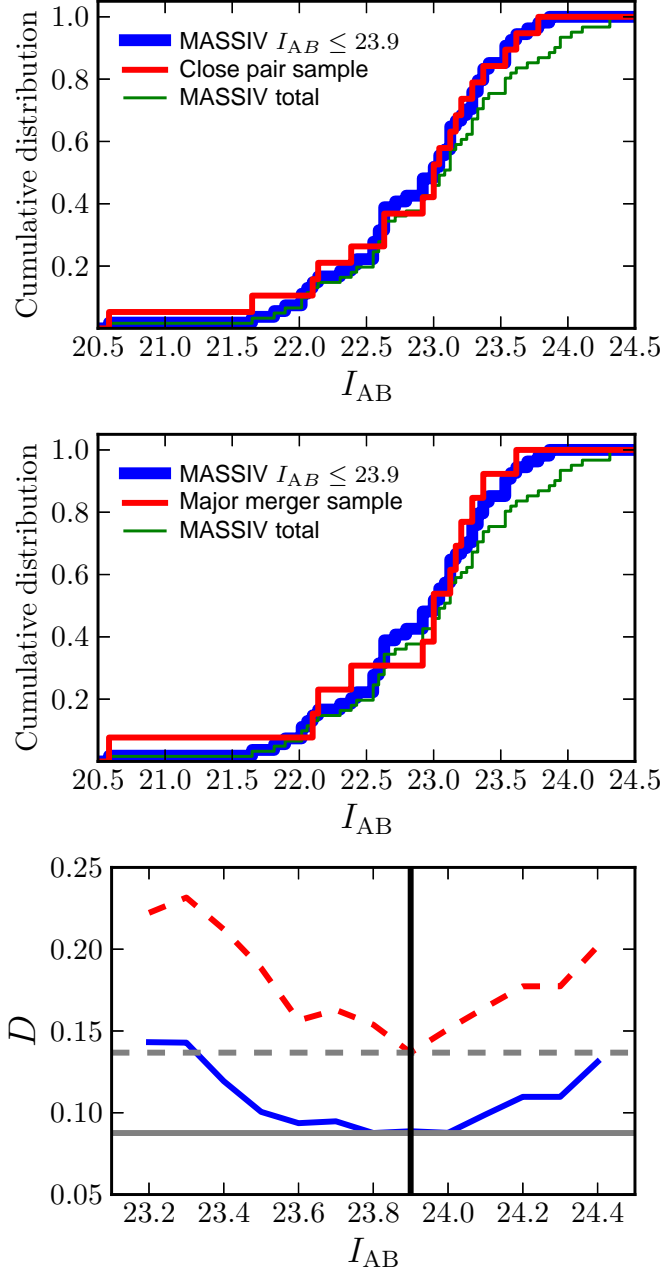


**Fig. C.1.** *Top*: cumulative distribution in the apparent  $I_{AB}$  magnitude of the total MASSIV sample (green line), the close pair sample (red line) and the total MASSIV sample with  $I_{AB} \leq 23.9$  (blue line). *Middle*: the same than before, but the red line shows the distribution of the major merger sample. *Bottom*: Kolmogorov-Smirnov estimator  $D$  of the total MASSIV sample distribution against the close pair (blue solid line) and the major merger (red dashed line) distributions. We computed  $D$  for those galaxies brighter than a given  $I_{AB}$  magnitude. The solid (dashed) horizontal line marks the minimum in the  $D$  distribution for close pairs (major mergers). The vertical solid line marks the  $I_{AB}$  magnitude at the minimum value of  $D$ ,  $I_{AB, \text{comp}} = 23.9$ . [A colour version of this plot is available at the electronic edition].